The Plant Cell, Vol. 22: 2476–2494, July 2010, www.plantcell.org 

# The Myosin Motor Domain of Fungal Chitin Synthase V Is Dispensable for Vesicle Motility but Required for Virulence of the Maize Pathogen *Ustilago maydis* [W]

**Steffi Treitschke,[a,b] Gunther Doehlemann,[b] Martin Schuster,[a] and Gero Steinberg[a,1]**

[a] School of Biosciences, University of Exeter, Exeter EX4 4QD, United Kingdom
[b] Max Planck Institute for Terrestrial Microbiology, D-35043 Marburg, Germany

**Class V chitin synthases are fungal virulence factors required for plant infection. They consist of a myosin motor domain fused to a membrane-spanning chitin synthase region that participates in fungal cell wall formation. The function of the motor domain is unknown, but it might deliver the myosin chitin synthase-attached vesicles to the growth region. Here, we analyze the importance of both domains in Mcs1, the chitin synthase V of the maize smut fungus *Ustilago maydis*. By quantitative analysis of disease symptoms, tissue colonization, and single-cell morphogenic parameters, we demonstrate that both domains are required for fungal virulence. Fungi carrying mutations in the chitin synthase domain are rapidly recognized and killed by the plant, whereas fungi carrying a deletion of the motor domain show alterations in cell wall composition but can invade host tissue and cause a moderate plant response. We also show that Mcs1-bound vesicles exhibit long-range movement for up to 20 μm at a velocity of ~1.75 μm/s. Apical Mcs1 localization depends on F-actin and the motor domain, whereas Mcs1 motility requires microtubules and persists when the Mcs1 motor domain is deleted. Our results suggest that the myosin motor domain of ChsV supports exocytosis but not long-range delivery of transport vesicles.**

## INTRODUCTION

Filamentous fungi are important pathogens on higher plants and are responsible for significant preharvest crop loss, causing an estimated annual cost of ~$30 billion only in the US (Pimentel et al., 2000). Invasion of the host plant by pathogenic fungi occurs by polar expansion of the fungal cell, a process known as hyphal tip growth (Steinberg, 2007). Tip growth requires continuous synthesis of fungal cell wall at the hyphal apex and is therefore based on the polar delivery of synthetic enzymes (Latge, 2007). Little is known about the mechanism by which enzyme-containing vesicles get delivered to the hyphal tip, but both filamentous actin and myosins, as well as actin regulators, like Cdc42 and Rac1, are crucial for plant infection (Weber et al., 2003; Fuchs et al., 2005; Chen et al., 2008; Zheng et al., 2009).

A major structural component of the fungal cell wall is chitin. This β-1,4-linked polymer of *N*-acetylglucosamine is synthesized by chitin synthases (CHSs), which are thought to be delivered in secretory vesicles to the growth region (Sietsma et al., 1996; Bartnicki-Garcia, 2006). Studies in numerous fungi have shown that the deletion of CHSs results in a weakening of the cell wall and causes abnormal growth of the fungal hyphae (Fujiwara et al., 1997; Horiuchi et al., 1999; Werner et al., 2007), as well as appressoria (Werner et al., 2007; Odenbach et al., 2009). Consequently, CHSs perform crucial roles in plant infection (e.g., Madrid et al., 2003; Garcera-Teruel et al., 2004; Martin-Udiroz et al., 2004, 2008; Soulie et al., 2006; Weber et al., 2006; Werner et al., 2007). They are therefore valuable targets for antimycotic drugs (Ruiz-Herrera and San-Blas, 2003). Genomes of filamentous fungi encode up to 10 CHSs (Miyazaki and Ootaki, 1997), which are grouped into seven classes (Choquer et al., 2004; Mandel et al., 2006; Nino-Vega et al., 2009), with classes III, V, and VII being typical for filamentous fungi. Out of these, classes V and VII CHSs contain an additional N-terminal myosin motor domain (MMD) fused to the C-terminal CHS domain. Class V CHSs (ChsV) are of particular interest because they are essential virulence factors in plant and human pathogens (Madrid et al., 2003; Liu et al., 2004; Weber et al., 2006; Werner et al., 2007; Kim et al., 2009). The CHS domain of the ChsV of *Ustilago maydis*, Mcs1, contains six predicted transmembrane domains that might insert the catalytic CHS core region into membranes of secretory transport vesicles. It is thought that upon fusion with the plasma membrane, the active site of CHSs participates in the formation of the extracellular fungal cell wall (Bartnicki-Garcia, 2006). The cytoplasmic N-terminal ~750 amino acids of class V and members of the related class VII CHSs show similarity to the motor domain of myosins (Fujiwara et al., 1997; Chigira et al., 2002; Takeshita et al., 2006; Nino-Vega et al., 2009), which are mechanoenzymes that hydrolyze ATP to perform mechanical work along filamentous actin (O'Connell et al., 2007). Due to their MMD, ChsVs are also considered to be myosin motors and are grouped as class XVII myosins (Hodge and Cope, 2000).

The MMD is essential for function and polar localization of CsmA and CsmB in *Aspergillus nidulans* (Takeshita et al., 2005;

[1] Address correspondence to g.steinberg@exeter.ac.uk.
The author responsible for distribution of materials integral to the findings presented in this article in accordance with the policy described in the Instructions for Authors (www.plantcell.org) is: Gero Steinberg (g.steinberg@exeter.ac.uk).
[W] Online version contains Web-only data.
www.plantcell.org/cgi/doi/10.1105/tpc.110.075028

Tsuizaki et al., 2009), and in analogy to the role of other myosins in membrane trafficking, it has been suggested that the motor domain participates in delivery of associated vesicles along actin filaments (F-actin) to the apical growth region (Fujiwara et al., 1997; Madrid et al., 2003; Abramczyk et al., 2009). Indeed, polar localization of CsmA, the class V CHS in *A. nidulans*, depends on F-actin (Takeshita et al., 2005). Furthermore, CsmA and CsmB bind F-actin in vitro, and this binding activity is required for polar localization (Takeshita et al., 2005; Tsuizaki et al., 2009). Conversely, a mutation in the ATP binding pocket of CsmA did not affect its polar localization, and it was therefore speculated that CsmA is delivered by a microtubule-based mechanism, whereas the MMD serves as an anchor for CsmA at the growth region (Takeshita et al., 2005). Microtubules, however, did not have a role in polar localization of Chs5p in *Wangiella dermatitidis* (Abramczyk et al., 2009), leaving the mechanism of delivery and the role of the MMD of class V CHSs elusive.

In this study, we focus on the class V CHS in the plant pathogen *U. maydis*. This basidiomycete smut fungus belongs to one of the largest group of plant pathogenic fungi, parasitizing on all relevant crop plants (Agrios, 1997). Previous work has shown that the class V CHS Mcs1 localizes to the cell tip of growing *U. maydis* hyphae where it is thought to participate in fungal cell wall formation (Weber et al., 2006). Mcs1 is dispensable for vegetative growth outside the plant but becomes essential during plant infection, with *mcs1*-null mutants swelling after entering the plant. It is currently not known whether the MMD participates in delivery of transport vesicles and if it is the CHS domain that is crucial for supporting cell wall synthesis during infection. Here, we combined live-cell imaging and plant infection assays to analyze the role of the domains of Mcs1 during pathogenic development. We find that both the CHS region and the MMD are important for Mcs1 function during plant infection. Mcs1 localization in the apical plasma membrane depends on F-actin as well as the motor domain. However, neither the MMD nor F-actin is crucial for delivery of Mcs1 to the hyphal tip. Instead, microtubules are required, indicating that associated kinesin motors are involved in tip-directed transport of myosin CHSs.

## RESULTS

### Polar Localization of Mcs1 Requires the Actin Cytoskeleton

It was previously reported that a fusion protein of yellow fluorescent protein and Mcs1 is functional and localizes to the growth region of yeast-like and hyphal cells of *U. maydis* (Weber et al., 2006). To visualize Mcs1 in infected plant tissue, we fused a triple tag of green fluorescent protein (GFP) to the N terminus of Mcs1. The fusion protein was introduced in single copy into the *ip* locus (Keon et al., 1991) of a solo-pathogenic *U. maydis* strain that was deleted in the endogenous *mcs1* gene (SG200ΔMcs1; see Table 1 for genotypes of all strains). When expressed under its native *mcs1* promoter, the 3xGFP-Mcs1 fusion protein ($G_3$Mcs1) rescued the ability of the deletion mutant to infect plants (see below), demonstrating its functionality. In agreement to previous reports, the fusion protein localized to the growing apex of invading hyphae within the plant (Figure 1A) and was predominantly concentrated at the periphery of the cell (Figure 1A, inset), suggesting its insertion in the apical plasma membrane. In axenic culture, $G_3$Mcs1 was also found at the growing apex (Figure 1B, arrowhead), but in addition occasionally accumulated in large organelles (Figure 1B, arrow) that colocalize with Cell-tracker blue and therefore most likely reflect degradation products in the vacuoles (see Supplemental Figure 1 online). To further characterize the relation between apical $G_3$Mcs1 signals and the plasma membrane, we fused monomeric Cherry (mCherry) to the N terminus of the putative *U. maydis* syntaxin Sso1 (accession number XP_760375). The encoded protein Sso1 shows 38% identity to *Saccharomyces cerevisiae* Sso1p, an integral syntaxin that functions at the plasma membrane (Aalto et al., 1993). In hyphal cells expressing both $G_3$Mcs1 and mCherry-Sso1, the majority of the myosin CHS colocalized with the plasma membrane (Figure 1C; see Supplemental Figure 2 online), and only few vesicles were observed in the apical cytoplasm (Figure 1C, inset, arrowhead). These vesicles might represent carriers that take Mcs1 to the growth region and could be so-called chitosomes (Bartnicki-Garcia, 2006). Integration of $G_3$Mcs1 into the plasma membrane was confirmed by immunogold labeling in electron microscopy studies using monoclonal and polyclonal anti-GFP antibodies. In these studies, we found that 46.5% ($n$ = 123) of the gold particles localized at the edge of the cytoplasm (Figure 1D), which is consistent with an insertion of Mcs1 into the plasma membrane. The remaining signals were found within the cortical 200 nm of the cytoplasm (34.2%) or even below (24.0%), indicating that a significant portion of the $G_3$Mcs1-bound vesicles concentrates beneath the plasma membrane.

Numerous reports describe a role of either F-actin or microtubules in delivery of class V CHSs to the hyphal apex (see Introduction). To address this question in our system, we applied the microtubule-destabilizing drug benomyl, the F-actin inhibitor latrunculin A (LatA), and the myosin inhibitor 2,3-butanedione monoxime at concentrations and conditions effective in *U. maydis* (Weber et al., 2003; Fuchs et al., 2005; see Methods). In control experiments, cells were treated with DMSO, the inhibitor solvent. We found that treatment with DMSO and benomyl did not drastically affect the apical localization of $G_3$Mcs1. In fact, without microtubules, Mcs1 seemed to be more concentrated in the plasma membrane and less dispersed (Figure 1E, Control and Benomyl). By contrast, the apical gradient was abolished when F-actin was disrupted by LatA (Figure 1E) or after inhibition of myosin activity by 2,3-butanedione monoxime (Figure 1E). This effect became most obvious in averaged quantitative line scan analyses of five hyphae (Figure 1F), which clearly demonstrate the loss of an apical concentration after inhibition of the acto-myosin system. These results argue for a role of the actin cytoskeleton in polar concentration of Mcs1.

### The MMD Is Essential for Polar Targeting of Mcs1

The inhibitor studies described above were in agreement with a putative function of the MMD of Mcs1 in the delivery process. To test this, we constructed numerous mutant alleles that were

**Table 1.** Strains and Plasmids Used in This Study

| SG200 | *a1 mfa2 bW2 bE* | Kämper et al. (2006) |
|---|---|---|
| SG200ΔMcs1 | *a1 mfa2 bW2 bE, Δmcs1::hyg$^R$, ble$^R$* | Weber et al. (2006) |
| SG200$G_3$Mcs1 | *a1 mfa2 bW2 bE, ble$^R$, Δmcs1::hyg$^R$*/pn3Mcs1 | This study |
| SG200$G_3$Mcs1mChSso1 | *a1 mfa2 bW2 bE, ble$^R$, Δmcs1::hyg$^R$*/pn3GMcs1/pomChSSO1 | This study |
| SG200$G_3$Mcs1ΔMM | *a1 mfa2 bW2 bE, bl$^R$e, Δmcs1::hyg$^R$*/pn3GMcs1ΔMM | This study |
| SG200$G_3$Mcs1noATP | *a1 mfa2 bW2 bE, ble$^R$, Δmcs1::hyg$^R$*/pn3GMcs1noATP | This study |
| SG200$G_3$Mcs1noact | *a1 mfa2 bW2 bE, ble$^R$, Δmcs1::hyg$^R$*/pn3GMcs1noAct | This study |
| SG200$G_3$Mcs1ΔCC | *a1 mfa2 bW2 bE, ble$^R$, Δmcs1::hyg$^R$*/pn3GMcs1ΔCC | This study |
| SG200$G_3$Mcs1noCHS | *a1 mfa2 bW2 bE, ble$^R$, Δmcs1::hyg$^R$*/pn3GMcs1noCHS | This study |
| FB2*crg*HAMcs1HN | *a2 b2*/p*crg*HAMcs1HN | This study |
| FB2*crg*HAMcs1H | *a2 b2*/p*crg*HAMcs1H | This study |
| pn3GMcs1 | P*mcs1-3xegfp-mcs1, cbx$^R$* | This study |
| pomChSSO1 | P*otef-mCh-sso1, nat$^R$* | This study |
| pn3GMcs1ΔMM | P*mcs-3xegfp-mcs1*$^{\Delta 57\text{-}753}$, *cbx$^R$* | This study |
| pn3GMcs1noATP | P*mcs-3xegfp-mcs1*$^{E407K}$, *cbx$^R$* | This study |
| pn3GMcs1noAct | P*mcs-3xegfp-mcs1*$^{\Delta 319\text{-}339}$, *cbx$^R$* | This study |
| pn3GMcs1ΔCC | P*mcs-3xegfp-mcs1*$^{\Delta 764\text{-}795}$, *cbx$^R$* | This study |
| pn3GMcs1noCHS | P*mcs-3xegfp-mcs1*$^{D1436E,\ D1551E}$, *cbx$^R$* | This study |
| pomChSSO1 | P*otef-mCh-sso1, nat$^R$* | This study |
| p*crg*HAMcs1HN | P*crg-HA-mcs1*$^{1\text{-}927}$*, cbx$^R$* | This study |
| p*crg*HAMcs1H | P*crg-HA- mcs1*$^{1\text{-}701}$*, cbx$^R$* | This study |

*a*, *b*, mating type loci; P, promoter; -, fusion; Δ, deletion; *hyg$^R$*, hygromycin resistance; *ble$^R$*, phleomycin resistance; *nat$^R$*, nourseothricin resistance; *cbx$^R$*, carboxin resistance; *crg*, conditional arabinose-induced promoter; /, ectopically integrated; *E1*, *W2*, genes of the *b* mating-type locus; *egfp*, enhanced green fluorescent protein; *mCh*, monomeric red fluorescent protein; Sso1, a syntaxin-like plasma membrane protein; Mcs1, Myosin-chitin synthase 1.

defective in the N-terminal motor domain (Figure 2A). These constructs included a deletion of the motor domain ($G_3Mcs1^{\Delta 57\text{-}753}$ = ΔMM), a deletion of a so-called myopathy loop that is required for actin binding in *A. nidulans* and *Dictyostelium discoideum* ($G_3Mcs1^{\Delta 319\text{-}339}$ = noAct; Sasaki et al., 1999; Takeshita et al., 2005), and an allele with a point mutation that has been shown to almost abolish ATPase activity of MyoA in *A. nidulans* and *D. discoideum* myosin ($G_3Mcs1^{E407K}$ = noATP; Liu et al., 2001). To investigate the importance of the CHS domain, a Mcs1-mutant protein was generated that contained two amino acid exchanges in the CHS core ($G_3Mcs1^{D1436E/D1551E}$ = noCHS). The mutated amino acids are conserved among CHSs and located in the active pocket, where they perform catalytic functions, shown to be essential for enzyme activity without affecting the substrate affinity (Nagahashi et al., 1995).

The C-terminal tail of Mcs1 is predicted to contain a coiled-coil region (Weber et al., 2006). In other myosins, such coiled-coil stretches were shown to support protein dimerization (Sellers, 2000). To test whether the Mcs1 dimerizes via this coiled-coil, we constructed truncated *mcs1* alleles with (HMcs1HN) and without the coiled-coil region, respectively (HMcs1H; see Supplemental Figure 3A online). We expressed the mutant proteins in *U. maydis* cells and performed gel filtration experiments to estimate their native size. While a large portion of both proteins eluted in the void volume, HMcs1HN also showed a strong peak at fractions 45 and 46 (~11.44 mL) and a second peak at fractions 50 and 51 (~12.69 mL). The truncated HMcs1H had a tendency to aggregate but was also detectable at a single peak at fraction 51 (see Supplemental Figure 3B online). By comparison with globular calibration proteins, the first peak of HMcs1HN represented a calculated protein size of ~240 kD, corresponding to the expected size of a Mcs1HN homodimer. By contrast, HMcs1H eluted at ~120 kD, which was the expected size for a monomer (see Supplemental Figure 3C online). The actual protein sizes of 216 kD (dimerized HMcs1HN) and 83 kD (monomeric HMcs1H) indicated dimerization of the Mcs1 motor head via the coiled-coil domain. To test the importance of dimerization for Mcs1 function, we generated a mutant protein lacking the coiled-coil domain ($G_3Mcs1^{\Delta 764-795}$ = ΔCC; Figure 2A). In analogy to the procedure described for $G_3$Mcs1 (see above), all constructs were integrated into the *ip* locus of a solo-pathogenic *mcs1*-null mutant and expressed under the native *mcs1* promoter. Quantitative immunoblot analysis revealed that all mutant proteins were expressed at similar levels (see Supplemental Figure 4 online). In hyphae, only $G_3$Mcs1 and the CHS defective noCHS mutant formed an apical gradient, while all other Mcs1 mutant proteins failed to accumulate at the growth region (Figure 2B, arrowheads). This suggests the motor domain of Mcs1 being crucial for delivery of Mcs1 to the apical plasma membrane.

## The CHS Domain and the Myosin Motor Head Are Necessary for Plant Pathology

The class V CHS Mcs1 is essential for plant infection, suggesting that its function is needed to support polarized growth during tissue invasion (Weber et al., 2006). We therefore performed plant infection assays to analyze the functional implications of the mutations and partial deletions in the motor domain, the coiled-coil region, and the CHS domain. When 7-d-old maize

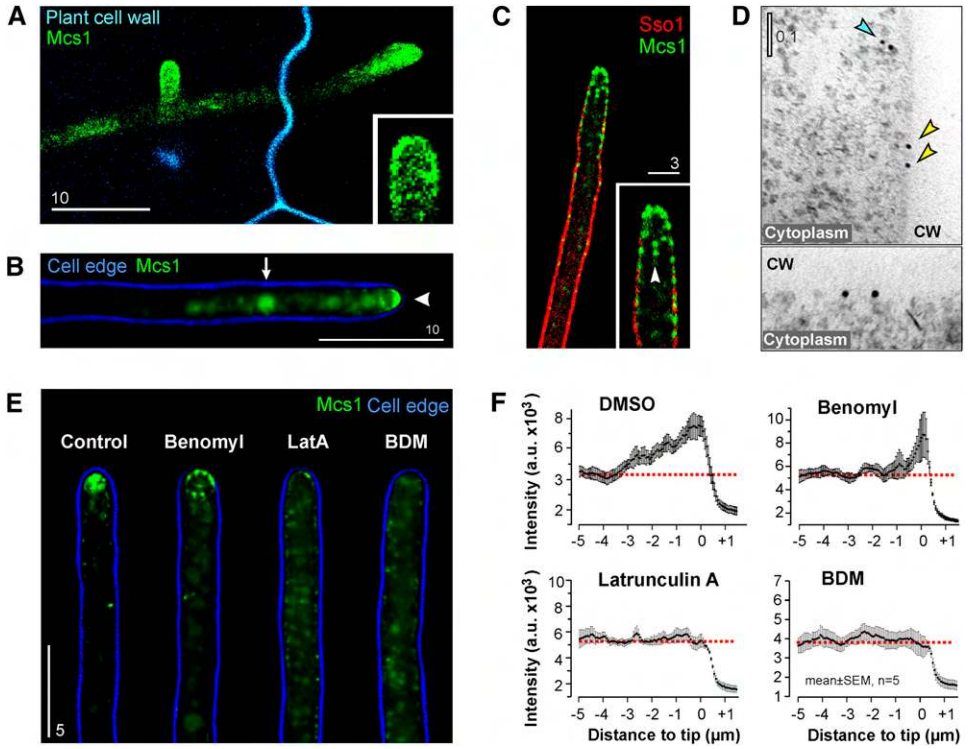


**Figure 1.** Localization of a Functional Mcs1 Fusion Protein Tagged with Triple GFP ($G_3$Mcs1).

**(A)** An infectious *U. maydis* hypha growing inside the plant host tissue. The $G_3$Mcs1 fusion protein (green) rescues the deletion phenotype of *mcs1* and localizes at the tip of the growing hypha. Autofluorescence of the plant cell wall is shown in blue. Bar represents micrometers.

**(B)** Localization of $G_3$Mcs1 (green) in infectious hyphae grown in axenic culture. The cell edge is indicated by an overlain false-color bright-field image (blue). The fusion protein concentrates at the hyphal growth region (arrowhead) and accumulates in vacuoles (arrow). Bar represents micrometers.

**(C)** Localization of $G_3$Mcs1 in the plasma membrane (red) and the apical cytoplasm of a hyphal cell. The plasma membrane was labeled by a fusion protein of an Sso1-like syntaxin fused to mCherry. Note that some signals are found in the apical cytoplasm (arrowhead in inset). Bar represents micrometers.

**(D)** Transmission electron micrographs showing immunogold labeling of $G_3$Mcs1 at the cell periphery. The majority of the signals localize at the edge of the cell where the plasma membrane is located (yellow arrowheads). In addition, a significant portion of the gold particles was found in the cortical 200 nm of the cell (blue arrowhead). The central cell region is almost free of label. CW, cell wall. Bar represents micrometers.

**(E)** Effect of cytoskeleton inhibitors on the localization of $G_3$Mcs1 in hyphae. The fusion protein (green) concentrates at the hyphal apex in the control (DMSO, the solvent of the inhibitors added at the same concentration as for the drug treatments) and benomyl (30 μM; microtubule-depolymerizing drug) treated cells (Benomyl). No apical concentration was found after 30 min in the presence of the F-actin inhibitor LatA (10 μM) or the myosin inhibitor 2,3-butandione monoxime (10 mM; BDM). Bar represents micrometers; the cell edge is indicated by an overlain false-color bright-field image (blue).

**(F)** Average signal intensity curves derived from line scans over five representative hyphae from one experiment; each data point represents mean ± SE. All results were confirmed by a second nonquantitative experiment.

(*Zea mays*) seedlings were infected with the solo-pathogenic progenitor strain SG200 (see Table 1 for genotype), large tumors on stems and leaves were observed 12 d after infection and many plants exhibited stunted growth (Figures 3A and 3B, WT). By contrast, plants infected with *mcs1*-null mutants showed no severe disease symptoms (Figures 3A and 3B, Δ*mcs1*), and only local chlorosis and necrotic spots were visible on infected leaves. Expression of $G_3$Mcs1 in Δ*mcs1* mutants largely restored virulence of the deletion phenotype, demonstrating functionality of the 3xGFP tagged Mcs1 protein (Figures 3A and 3B, Control). Although localizing at the growth region (see above), the noCHS mutant did not rescue virulence of the deletion mutant (Figures 3A and 3B, noCHS), suggesting that the CHS domain of Mcs1 is of crucial importance for plant infection. When the MMD was deleted or mutated, only few and small tumors developed on infected leaves (Figures 3A and 3B, ΔMM, noAct, and noATP). Thus, the MMD is important for full virulence of *U. maydis*, but it is not essential for pathogenic development. Surprisingly, deletion of the coiled-coil region located C-terminally of the motor domain almost abolished development of disease symptoms in maize (Figures 3A and 3B, ΔCC), suggesting that dimerization is of particular importance for Mcs1 function.

### Mutants in the MMD Exhibit Morphological Defects in Planta

The intermediate phenotype of mutants in the MMD prompted us to investigate the infection process on the cellular level. To this end, samples of infected leaf tissue of control and mutant strains

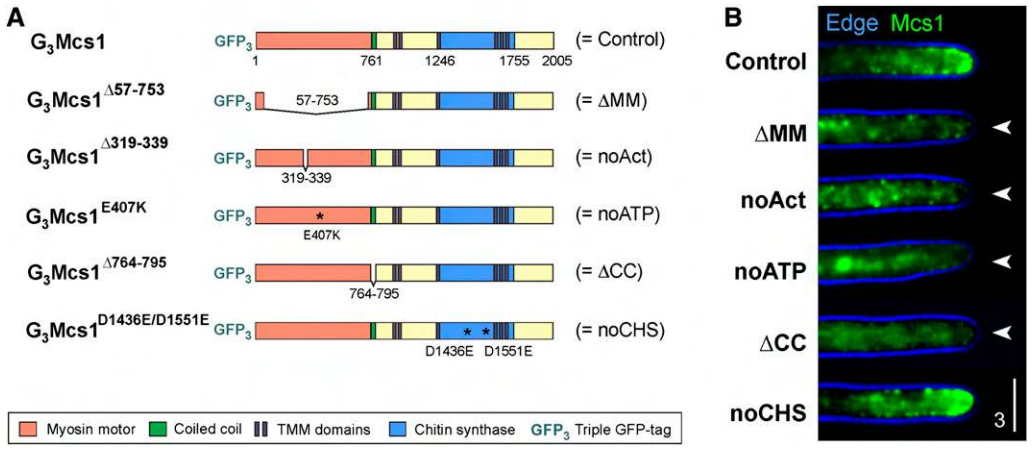


**Figure 2.** $G_3$Mcs1 Mutant Proteins Defective in the Motor Domain or the CHS Region.

**(A)** Diagram depicting the domain organization of $G_3$Mcs1 (Control) and numerous mutant proteins either lacking the MMD ($G_3Mcs1^{\Delta 57\text{-}753}$; ΔMM) or a loop involved in actin binding ($G_3Mcs1^{\Delta 319\text{-}339}$; noAct) or carrying a point mutation in the motor domain that impairs ATPase activity ($G_3Mcs1^{nE407K}$; noATP), a deletion of a region that is predicted to form a coiled-coil ($G_3Mcs1^{\Delta 764\text{-}795}$; ΔCC), or point mutations that abolish the putative CHS activity ($G_3Mcs1^{D1436E/D1551E}$; noCHS). Numbers indicate amino acid position of the respective mutations.

**(B)** Localization of control and mutant proteins in infectious hyphae grown in axenic culture. The localization of the GFP fusion proteins is shown in green; the cell edge is indicated by an overlain false-color bright-field image (blue). All mutations in the motor domain abolished polar accumulation (arrowheads). Bar represents micrometers.

were taken 3 d after infection and prepared for visualization of fungal hyphae and the plant cell wall (see Methods). In control experiments using cells expressing $G_3$Mcs1, hyphae were found to proliferate within the entire plant leaf (Figure 4A, Control). This behavior was not distinguishable from infections with the progenitor strain SG200 (data not shown). In agreement with previous reports, almost no colonization of plant tissue was found after infections with Δ*mcs1* mutants (Figure 4A, Δ*mcs1*). A similar phenotype was observed in mutants lacking CHS activity (Figure 4A, noCHS) and mutants deleted in the coiled-coil region (Figure 4A, ΔCC). By contrast, mutations within the MMD, including deletion of the complete domain, did not abolish plant invasion by the fungus (Figure 4A, ΔMM, noATP, and noAct). Hyphae of these mutants were found to colonize the maize leaf tissue; however, infection remained local and restricted to few cells.

To assess the differences in plant colonization in a quantitative way, the relative fungal amount in infected plant leaves was calculated using quantitative real-time PCR by comparing the relative amount of fungal to plant DNA (see Methods). In agreement with the microscopy analysis, *mcs1*-null mutants expressing $G_3$Mcs1 showed almost SG200 infection levels (Figure 4B, Control), whereas only very little fungal DNA was detected in the absence of Mcs1 (Figure 4B, Δ*mcs1*) or after infection with cells expressing a fusion protein containing mutations in the CHS core region (Figure 4B, noCHS). Consistent with the microscopy results, the motor domain mutants showed an intermediate degree of colonization (Figure 4B, ΔMM, noAct, and noATP).

Mcs1 is a CHS that is supposed to participate in cell wall formation during invasive growth. Deletion mutants were reported to swell and display severe morphological defects (Weber et al., 2006). Therefore, we analyzed whether the intermediate phenotype of the MMD mutants correlates with reduced morphological defects. In agreement to previous reports, we found that Δ*mcs1* mutant hyphae were swollen and irregular (Figure 5A, Δ*mcs1*; see Supplemental Movie 1 online), which was in striking contrast to the thinner and regularly branched control and $G_3$Mcs1 hyphae (Figure 5A, WT and Control; see Supplemental Movie 2 online). The morphological phenotypes of mutants expressing ΔCC and noCHS were similar to that of *mcs1*-null mutant. By contrast, motor domain mutants were more regular, with thinner hyphae and less severe swellings (Figure 5A, ΔMM, noAct, and noATP; see Supplemental Movie 3 online). However, they seem to be hyperbranched and consisted of shorter cells. To quantify these morphological phenotypes, the number of hyphae showing spherical swellings within the apical 10 μm, the hyphal diameter in subapical regions and the variability of the hyphal diameter were measured (Figure 5B). This analysis demonstrated that SG200 and control cells show only little variation in all parameters analyzed, whereas both Δ*mcs1* and noCHS mutants exhibited similar morphological defects. Again, expression of ΔMM, noATP, and noAct resulted in an intermediate phenotype (Figure 5B). Taken together, these results suggest that the CHS activity of Mcs1 is crucial for morphology of *U. maydis* hyphae during plant infection. Although the MMD is needed for full virulence and hyphal morphology, it is not essential for tip growth inside the plant.

### Reduction of Pathogenicity in Mcs1 Mutants Correlates with Reduced $H_2O_2$ Accumulation

Increasing evidence suggests that *U. maydis* actively suppresses the plant defense to establish biotrophy and colonize the host tissue (Kämper et al., 2006). A possible explanation for the pathogenicity defect of *mcs1*-null mutants would be that they are

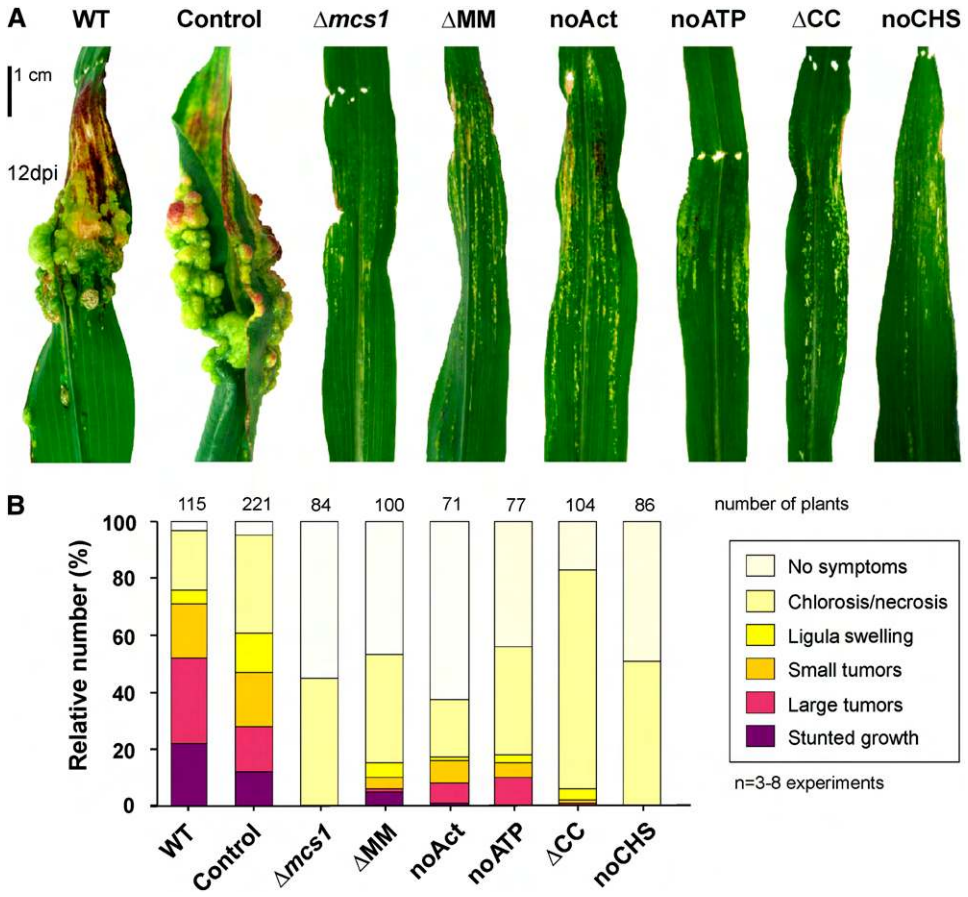


**Figure 3.** Plant Disease Symptoms after Infection with *U. maydis* Wild-Type and Deletion Mutants Expressing $G_3$Mcs1 and Mutant Proteins.

**(A)** Symptoms on maize leaves infected with progenitor strain SG200 (WT), a *mcs1*-deletion mutant (Δ*mcs1*), and Δ*mcs1* mutants expressing $G_3$Mcs1 (control) and various mutant proteins (for nomenclature, see Figure 2A). Wild-type and control strains induce tumors, whereas mutants in the MMD show only local necrotic regions. Very little disease symptoms were found in Δ*mcs1* and mutants defective in the CHS region (noCHS).

**(B)** Quantitative analysis of plant symptoms 12 d after infection with wild-type strain SG200 (WT), a *mcs1*-deletion mutant (Δ*mcs1*), and Δ*mcs1* mutants expressing $G_3$Mcs1 (control) and various mutant proteins. Note that the deletion of the coiled-coil region (ΔCC) almost abolishes function of the myosin CHS. Quantitative data represent 71 to 221 plants analyzed in three to eight experiments.

unable to avoid plant responses and are therefore killed by plant defense mechanisms including oxidative burst and the hypersensitive reaction. To test this hypothesis, we visualized the presence of $H_2O_2$ using diaminobenzidine (DAB), which reacts with local $H_2O_2$, resulting in a reddish-brown colored precipitate (Thordal-Christensen et al., 1997; Liu et al., 2007). Infections with control hyphae expressing $G_3$Mcs1 result in a very faint color reaction (Figures 6A and 6B, Control). When this reaction was visualized in false-colored images, it became apparent that this occurrence was restricted to the growing hyphal tip (see Supplemental Figure 5A online; Control). This suggests that invading hyphae become invisible to the plant defense system during intracellular growth due to cell wall maturation. By contrast, deletion of Mcs1 causes a much stronger accumulation of $H_2O_2$ (Figures 6A and 6B, Δ*mcs1*). A similar degree of DAB oxidation was seen in mutants expressing noCHS (Figures 6A and 6B, noCHS), again suggesting that defects in the cell wall trigger an oxidative burst. By contrast, deletion or mutation of the motor domain in Mcs1 resulted in a weaker reaction and less DAB staining (Figures 6A and 6B, ΔMM). Again, the reaction was most prominent at the tip of slightly thickened and hyperbranched hyphae (see Supplemental Figure 5A online, ΔMM, arrowheads).

It was shown that cell wall components like α(1,3)-glucan, a homopolymer of glucose with α-glycosidic linkages, or chitosan, a deacetylated form of chitin, protect invading fungal hyphae against recognition by the host defense system (O'Connell and Panstruga, 2006; Rappleye et al., 2007; Fujikawa et al., 2009). The increased $H_2O_2$ production in planta suggested that *mcs1* mutants are unable to avoid a plant response due to alterations in these protective (masking) cell wall polysaccharides. To test this hypothesis, infective hyphae were incubated with an antibody specific for α(1,3)-glucan (Rappleye et al., 2007; Fujikawa et al., 2009). This antibody bound to the surface of hyphae expressing $G_3$Mcs1 (Figure 6C, control; see Supplemental Figure 6 online) but did not bind to $G_3Mcs1^{\Delta 57\text{-}753}$–expressing cells (Figure 6C, ΔMM) or to *mcs1*-null mutants (see Supplemental Figure 6

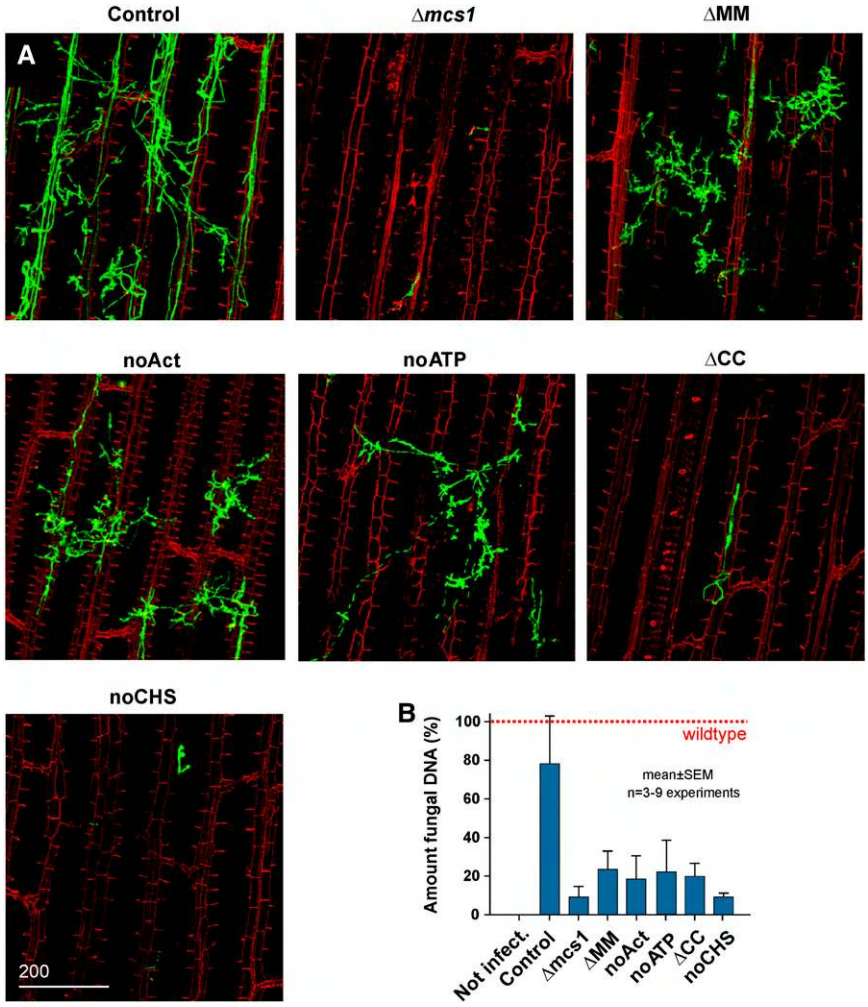


**Figure 4.** Histology of Plant Infection by *mcs1* Mutants.

**(A)** Fungal material is labeled by WGA/AF488 (green), and the plant cell wall is marked with propidium iodide (red). The *mcs1* deletion mutants (Δ*mcs1*) only rarely proliferate within the plant, whereas expression of $G_3$Mcs1 (control) enables colonization of the leaf tissue. Expression of proteins defective in the MMD (ΔMM, noAct, and noATP) allows the mutant to spread locally within the tissue, but the infection remains regional. Almost no infection was found when the coiled-coil region was deleted (ΔCC) or when the CHS activity was abolished (noCHS). Bar represents micrometers.

**(B)** Bar chart showing the relative amount of fungal biomass in infected plant leaf tissue. Only little fungal DNA was detected in *mcs1*-null mutant and in mutants defective in CHS activity (noCHS). Slightly more fungal amount was amplified from mutants defective in the MMD of Mcs1. All bars are given as mean ± SE of three to nine independent infection experiments.

online). This strongly suggests that α(1,3)-glucan levels are reduced in the cell wall in *mcs1* mutants. Unfortunately, this labeling method was not suitable to detect hyphal α(1,3)-glucan in planta, and we therefore aimed to visualize fungal cell wall–bound chitosan, which can be specifically stained by the small molecule EosinY (Baker et al., 2007). Epidermal peels of *U. maydis* infected plants were used for fixation and subsequent incubation with EosinY. In samples infected with a control strain expressing $G_3$Mcs1, invasive hyphae were clearly stained by the dye (Figure 6D). By contrast, hyphae expressing $G_3Mcs1^{\Delta 57\text{-}753}$ (ΔMM) showed only a faint, marginal staining. Quantitative analysis of the background-corrected fluorescence signal in randomly selected hyphae confirmed a significant reduction of EosinY staining (Figure 6E). Together, these results show that mutations in the MMD of Mcs1 cause alterations in the cell wall composition and reduce the abundance of protective cell wall polymers.

Recognition of an invading hypha is often followed by a hypersensitive reaction and local cell death, which isolates and kills the attacking pathogen (Lamb and Dixon, 1997). We checked in living cells for reorganization of internal membranes and disintegration of plant cells by staining plant membranes with FM4-64 (Doehlemann et al., 2008); fungal material on the plant surface or in disintegrated plant cells was visualized with fluorescent wheat germ agglutinin (WGA/AF488). In control experiments using plants infected with $G_3$Mcs1-expressing

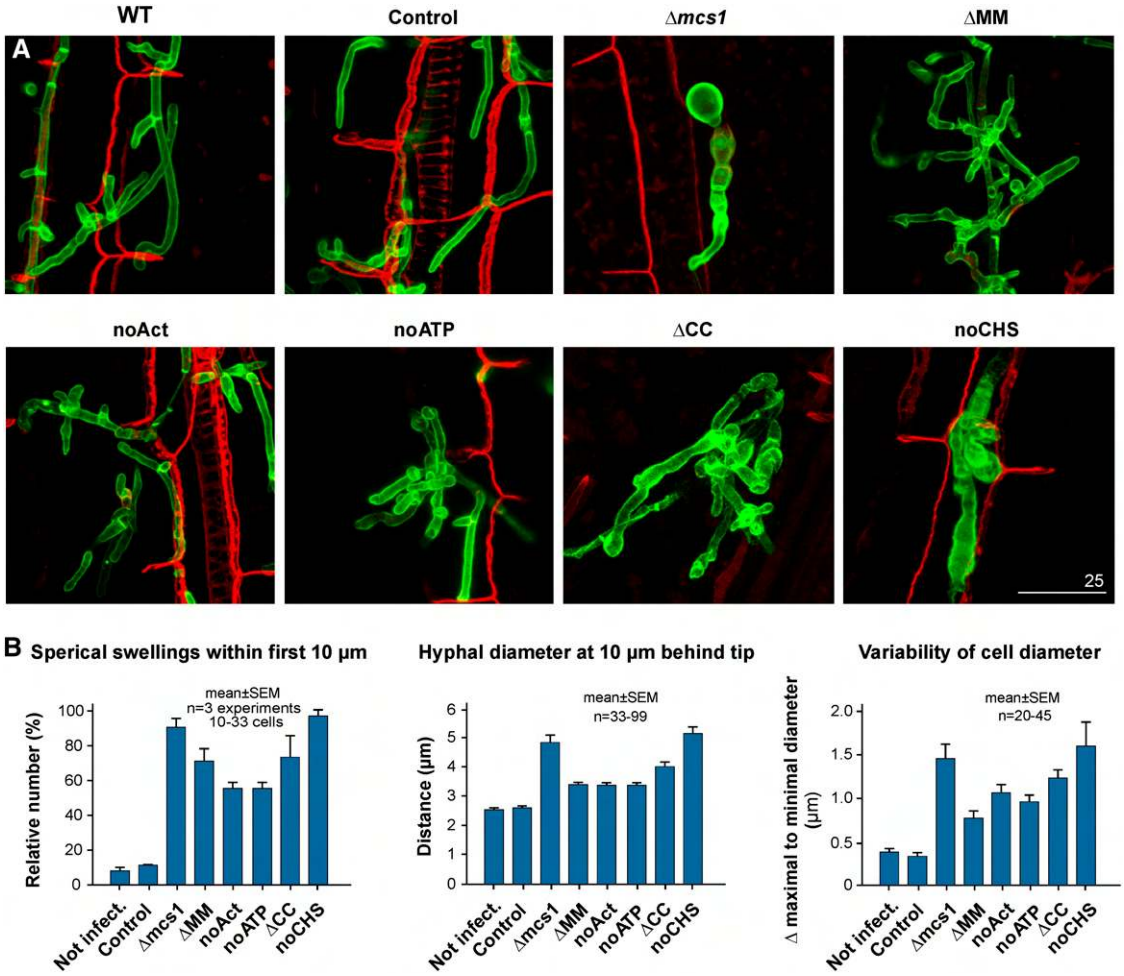


**Figure 5.** Morphology of *mcs1* Mutants 3 d after Infection.

**(A)** Both SG200 (WT) and *mcs1*-deletion mutants expressing $G_3$Mcs1 (control) colonize the plant by invasive growth and form branching hyphae. The *mcs1* deletion mutant and the CHS activity defective mutant (noCHS) display swollen and enlarged cells. Mutants deleted or mutated in the MMD show thicker and more branched hyphae. Fungal material is labeled by WGA/AF488 (green), and the plant cell wall is marked with propidium iodide (red). Bar represents micrometers.

**(B)** Bar charts showing quantitative evaluation of morphometric parameters, including hyphal swellings and average and variability of the hyphal cell diameter. In all parameters tested, SG200 (WT) and control show no differences. The *mcs1*-null mutant (Δ*mcs1*) and the mutant with abolished CHS activity (noCHS) displayed the most severe phenotype. Again, mutants in the MMD show an intermediate phenotype (ΔMM, noATP, and noAct). All bars are given as mean ± SE of 10 to 99 cells measured in three independent infection experiments.

mutants, intracellular hyphae where surrounded by a FM4-64–labeled plant membrane and could not be stained by the water soluble WGA/AF488 (arrowheads in Figure 6F, Control), demonstrating that the plant cell is alive and intact. By contrast, penetration of *mcs1*-null mutants (Figure 6F, Δ*mcs1*) or MMD mutants (see Supplemental Figure 5B online) resulted in granular FM4-64 staining and a condensation of the plant protoplast (best seen in Supplemental Figure 5B online, noCHS), suggesting that internal membrane organization is affected and integrity of the plant plasma membrane is no longer maintained. This might indicate cell death (Doehlemann et al., 2008) but also could reflect increased endocytic activity of the plant cell due to pathogen attack. In summary, these data show that all mutations in Mcs1 trigger an increased $H_2O_2$ production that is followed by local plant cell death. However, the degree to which the plant reacts differs between the mutants, with defects in the CHS domain eliciting the strongest reaction of the plant defense system.

### The MMD Is Not Required for $G_3$Mcs1 Motility

The results described so far demonstrate the importance of the Mcs1 motor domain for polar targeting of the class V CHS to the growth region. Assuming that the motor domain of Mcs1 delivers its own CHS domain, both regions should be of equal importance. However, our data showed this not being the case. To

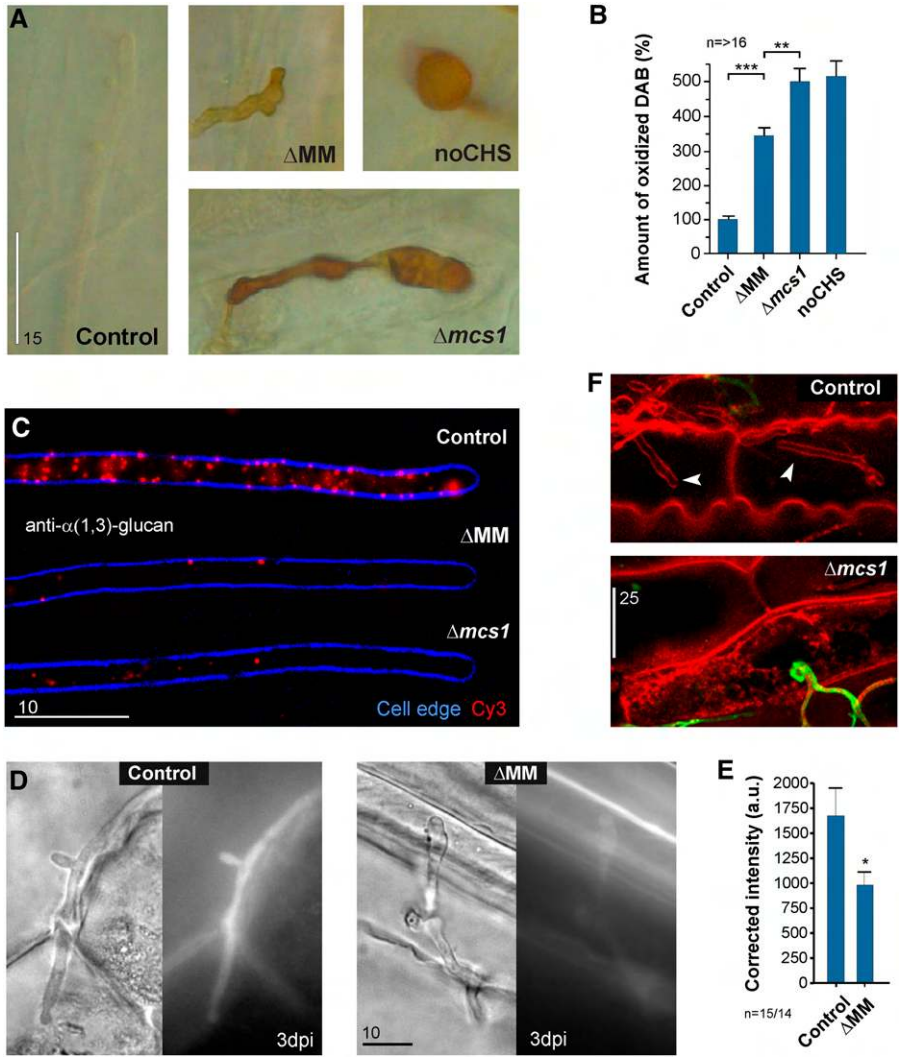


**Figure 6.** Oxidative Burst and Hypersensitive Reaction in Plant Leaves 36 h after Infection.

**(A)** and **(B)** Reddish-brown precipitate of oxidized DAB indicates the presence of $H_2O_2$. Only a little DAB precipitation was detected in plants 36 h after infection with *mcs1*-null mutants that express $G_3$Mcs1 (control). By contrast, an intense color reaction was characteristic for mutants expressing Mcs1 lacking the MMD (ΔMM) or mutants impaired in CHS activity (noCHS). Cells that express ΔMM showed an intermediate reaction, indicating that the plant defense is less severe. Bar in **(A)** represents micrometers; error bars in **(B)** represent SE. Double asterisk indicates significance at $P < 0.001$; triple asterisks indicate significance at $P < 0.0001$ (Student's *t* test). All bars are given as mean ± SE of at least 16 cells from two independent infection experiments. All values were corrected for background.

**(C)** Staining of α(1,3)-glucan in the cell wall of Δ*mcs1* hyphae expressing $G_3$Mcs1 (Control) and $G_3Mcs1^{\Delta 57\text{-}753}$ (ΔMM) or *mcs1*-null mutants (Δ*mcs1*). The cell edge is indicated by an overlain false-color bright-field image (blue), and dots represent Cy3-conjugated secondary antibody (red). Bar represents micrometers.

**(D)** EosinY staining of chitosan in cells expressing $G_3$Mcs1 (Control) and $G_3Mcs1^{\Delta 57\text{-}753}$ (ΔMM) in planta 3 days after infection (3dpi). Control cells expose more chitosan that might protect them against the plant defense system. Bar represents micrometers.

**(E)** Bar chart showing quantification of EosinY-stained chitosan in Δ*mcs1* cells expressing $G_3$Mcs1 (Control) and $G_3Mcs1^{\Delta 57\text{-}753}$ (ΔMM) expressing hyphae in planta 3 d after infection (3dpi). Asterisk indicates significance at $P < 0.05$. All bars are given as mean ± SE of 20 to 45 cells from one infection experiments. All results were confirmed by a second nonquantitative experiment. All values were corrected for background.

**(F)** Infection structures of *U. maydis* control hyphae at 36 h after infection (Control). Fungal hyphae are surrounded by the plant plasma membrane stained with FM4-64 (arrowheads). Penetration of *mcs1*-null mutant hyphae (green) induced changes in the membrane organization of the plant cell (Δ*mcs1*). Bar represents micrometers.

address this contradiction, we aimed to visualize the delivery of Mcs1-bound vesicles to the hyphal tip. We used a 488-nm laser light to excite GFP, which increased the sensitivity of the microscopy setup and allowed detection of fluorescent signals at low exposure. This enabled visualization of $G_3$Mcs1 in the plasma membrane within the apex but also in subapical parts of the hypha (Figure 7A, Control). Surprisingly, $G_3$Mcs1$^{\Delta 57\text{-}753}$ was found in the plasma membrane as well (Figure 7A, ΔMM, inset), although a quantitative analysis of background-corrected intensities demonstrated that significantly less $G_3$Mcs1$^{\Delta 57\text{-}753}$ was exposed at the cell surface (Figures 7B and 7C; dotted line in 7B indicates area of measurement). The presence of the truncated Mcs1 protein within the plasma membrane indicated additional and Mcs1 motor domain–independent mechanisms for delivery. To address the delivery process more directly, we set out to visualize the motility of individual $G_3$Mcs1 signals in living hyphae. To reduce the cytoplasmic background, we photobleached apical parts of the hypha (Figure 7D) using 405-nm laser light. We observed $G_3$Mcs1 signals moving into the darkened region of the hypha at a velocity of 1.74 ± 0.35 μm/s ($n$ = 35; see Supplemental Movie 4 online). This motility was persistent and did often last over >10 μm (Figure 7E, Control). Surprisingly, similar motility was found in cells expressing $G_3$Mcs1$^{\Delta 57\text{-}753}$ (Figure 7F, ΔMM). These results clearly demonstrate that Mcs1-bound vesicles move over long distances toward the hyphal apex in a Mcs1 motor domain–independent way. We next tested the role of the cytoskeleton in this motility and treated hyphae with the microtubule disrupting drug benomyl and the F-actin inhibitor latrunculin A. Surprisingly, we found that motility was abolished in the absence of microtubules (Figure 7G, Benomyl), whereas motility was still detected when F-actin was disrupted (Figure 7G, LatA). However, the degree of motility was significantly reduced in the absence of F-actin (Figure 7H), suggesting that myosin motors might also participate in the delivery of Mcs1.

The outcome of these experiments suggests that the transport mechanism involves microtubules. To confirm this, we tested the dynamics of Mcs1 at the hyphal apex using fluorescence recovery after photobleaching. At first, $G_3$Mcs1 was photobleached in DMSO and benomyl-treated cells, and signal recovery due to delivery of unbleached $G_3$Mcs1 was monitored. Consistent with a role of microtubules in delivery of $G_3$Mcs1, recovery of the Mcs1 accumulation was almost abolished in the presence of benomyl (Figures 8A and 8B). Next, the complete hyphal cell was photobleached without affecting the tip-bound $G_3$Mcs1 accumulation. In control cells, the signal at the tip rapidly decreased, whereas it remained largely unaffected in cells treated with benomyl (Figures 8C and 8D). These results demonstrate that microtubules are required for anterograde as well as retrograde transport of Mcs1.

## DISCUSSION

### The CHS Domain Is Essential for Pathogenicity

Class V CHSs have been shown to play important roles for pathogenicity of *Fusarium oxysporum*, *Gibberella zeae*, *Colletotrichum graminicola*, *Wangiella dematitidis*, as well as in the maize smut fungus *U. maydis* (Madrid et al., 2003; Liu et al., 2004; Weber et al., 2006; Werner et al., 2007; Kim et al., 2009). However, all these studies have analyzed phenotypes of CHS deletion mutants. Therefore, it remained elusive how the different parts of the myosin CHS protein contribute to pathogenicity. Assuming the Mcs1 MMD participates in polar delivery of Mcs1-bound vesicles (see below), two scenarios are possible: first, the CHS activity of Mcs1 might be crucial during plant invasion by maintaining integrity of the fungal cell wall. Alternatively, the integral membrane protein Mcs1 might deliver transport vesicles, containing unknown additional factors, such as secreted enzymes, which are essential to support plant invasion. We tested these hypotheses by mutating two crucial amino acids in the CHS core region, thereby leaving the MMD functionally intact. These modifications have been reported to abolish the enzymatic activity of Chs2 in *S. cerevisiae* (Nagahashi et al., 1995). As expected, the mutated protein localized correctly to the growth region, suggesting the delivery mechanism was not affected. However, in all parameters tested, *mcs1*-null and CHS impaired mutants were phenotypically indistinguishable. Therefore, we considered it most likely that the severe reduction in virulence in *mcs1*-null mutants is due to a lack of the Mcs1 CHS activity. However, this does not exclude the possibility that other pathogenicity factors are passively traveling in Mcs1-bound vesicles. One candidate could be CHS 6, which was shown to be essential in virulence of *U. maydis* (Garcera-Teruel et al., 2004). Alternatively, secreted effectors that protect the fungus from the plant defense system (Kämper et al., 2006) might get delivered by the Mcs1-bound vesicles. Proteomic approaches on purified transport vesicles will be necessary to address this question.

### Infection of Mcs1-Defective Mutants Is Stopped by Plant Defense

Plants are continuously challenged by a wealth of different pathogens that, in most cases, are successfully parried by the immune system that efficiently recognizes nonadapted pathogens. A rapid plant defense reaction is the so-called oxidative burst, which constitutes the production of reactive oxygen species that directly attack the fungal cell wall but also trigger subsequent plant cell death (Levine et al., 1994; Lamb and Dixon, 1997). *U. maydis* establishes a compatible, biotrophic interaction with maize and colonizes living plant cells, while defense responses are actively suppressed (Brefort et al., 2009). In our experiments, $G_3$Mcs1-expressing control hyphae caused a minor defense reaction at the hyphal tip. However, no $H_2O_2$ accumulation was found along the subapical parts of the hypha, indicating that cell wall maturation participates in the formation of a biotrophic interface. Abnormal growing *mcs1*-null mutants induced a strong plant reaction, and the severely swollen hyphae were no longer able to maintain a focused growth region. A similar morphological phenotype has also been described for CHSV-null mutants in *C. graminicola* (Werner et al., 2007). One might argue that the morphological defect of in planta growing hyphae of *mcs1*-null mutants in *U. maydis* is a result of the strong plant defense response. However, a *U. maydis* null mutant in *yap1*, a central regulator of oxidative stress responses, also

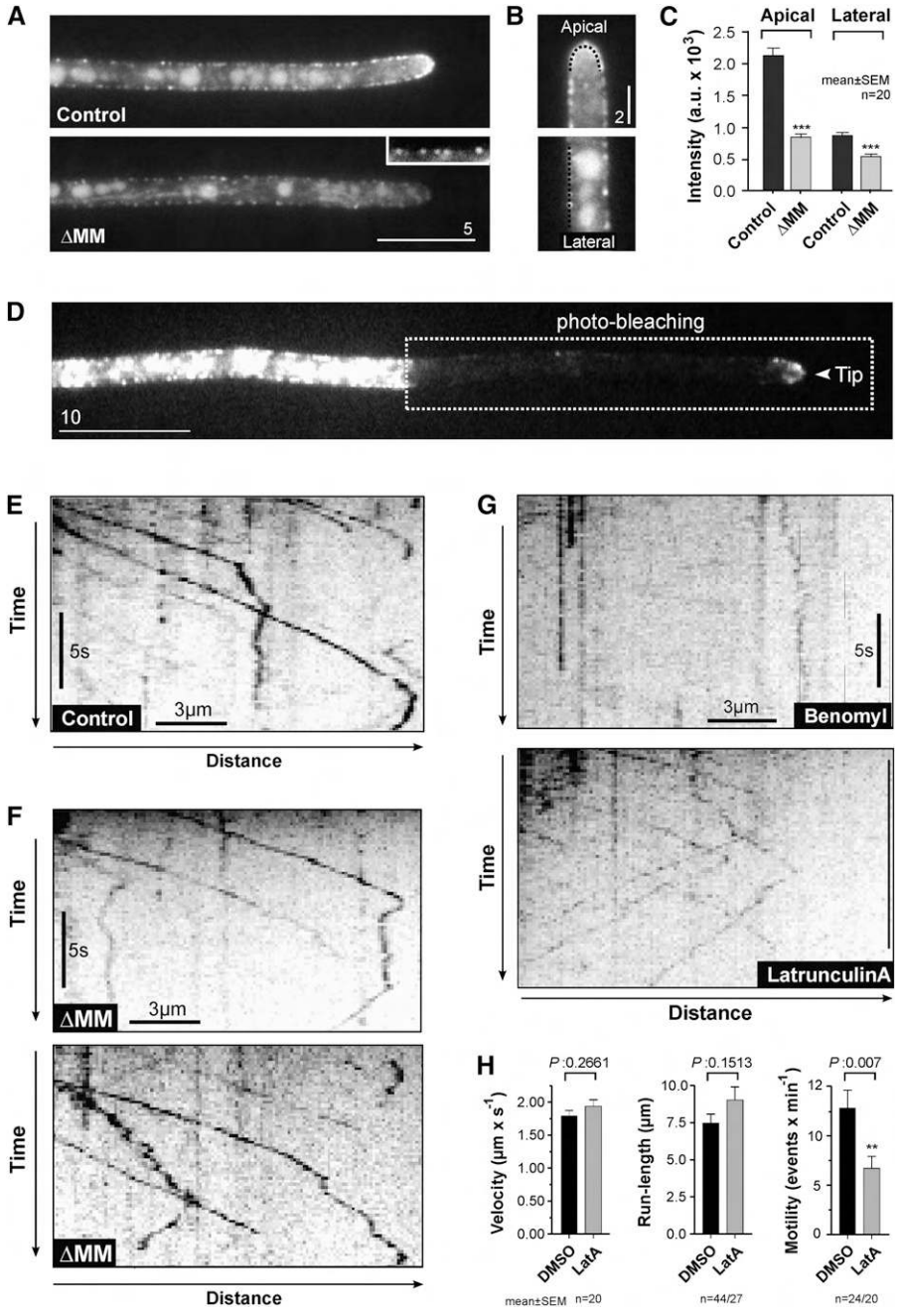


**Figure 7.** Motility of $G_3$Mcs1 and $G_3Mcs1^{\Delta MM}$.

**(A)** *mcs1*-null mutant hyphae expressing Mcs1-GFP fusion, $G_3$Mcs1 (Control), and $G_3Mcs1^{\Delta 57\text{-}753}$ (ΔMM). Even in the absence of the MMD, $G_3Mcs1^{\Delta 57\text{-}753}$ localizes to the plasma membrane at the cell periphery (inset). Bar represents micrometers.

**(B)** Images showing the region where intensity measurements were taken (dotted line) at the hyphal apex (Apical) and in subapical regions (Lateral). Bar represents micrometers.

**(C)** Bar chart showing the average intensity in the cell periphery within the apex (Apical) and 5 to 10 μm behind the cell tip (Lateral). In the absence of the motor domain (ΔMM), significantly less Mcs1 localizes in the plasma membrane. Triple asterisks indicate significance compared with control at $P < 0.0001$ (Student's *t* test). All bars are given as mean ± SE of 20 cells from two experiments. All values were corrected for background.

**(D)** Example of a *mcs1*-null hypha expressing $G_3$Mcs1. Photobleaching of the apical part of the hypha by photobleaching with a 405-nm laser reduces background and allows observation of $G_3$Mcs1-bound vesicles moving into the bleached apical region. Cell tip indicated by arrowhead. Photobleached area indicated by box.

**(E)** A graphical representation of spatial position over time (Kymograph) showing tip-directed motility of $G_3$Mcs1-bound vesicles. Moving signals appear

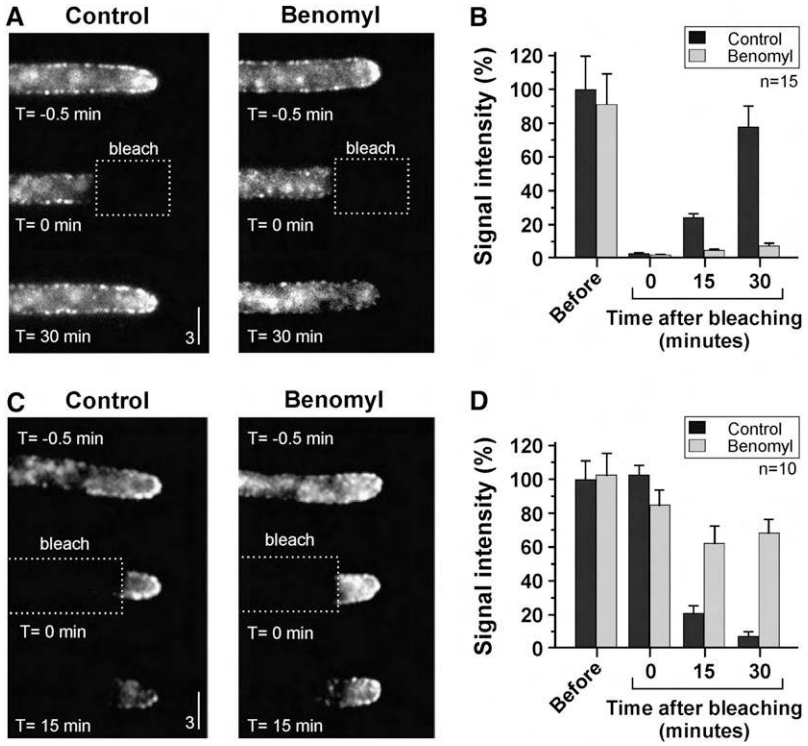


**Figure 8.** Dynamics of Apical Mcs1 after Photobleaching

**(A)** Recovery of $G_3$Mcs1 signals at the apex of fungal hyphae after photobleaching with a 405-nm laser. The apical accumulation recovers in the presents of the solvent DMSO (Control) but does not return in the absence of microtubules (Benomyl). Bar represents micrometers.

**(B)** Bar chart showing average $G_3$Mcs1 signal intensity at the hyphal tip before and at different time points after photobleaching. All bars are given as mean ± SE of 15 cells from one experiment. All values were corrected for background. All results were confirmed by a second nonquantitative experiment.

**(C)** Decay of $G_3$Mcs1 signals at the apex of fungal hyphae after photobleaching subapical parts using a 405-nm laser. Within 15 min the apical accumulation decays in the solvent DMSO (Control). In the absence of microtubules (Benomyl), the decay is significantly impaired. Bar represents micrometers.

**(D)** Bar chart showing decay of average $G_3$Mcs1 signal intensity at the hyphal tip before and at different time points after photobleaching. All bars are given as mean ± SE of 10 cells from one experiment. All values were corrected for background. All results were confirmed by a second nonquantitative experiment.

triggers an oxidative burst and plant cell death, without affecting hyphal morphology (Molina and Kahmann, 2007). We therefore consider it more likely that deletion or inactivation of Mcs1 results in alterations in fungal cell wall composition. This could affect cell wall integrity and might cause the observed morphological aberrations, including a loss in hyphal polarization. As a consequence, disturbed hyphal growth will decelerate fungal proliferation within the host tissue and might inhibit spreading within the plant tissue. Moreover, the defect in chitin incorporation into the cell wall is likely to result into an altered surface composition of *mcs1* mutant hyphae, which is recognized by the plant defense system. The reduced levels of α(1,3)-linked glucose and chitosan in the cell wall of *mcs1* mutant strains support this assumption. Both cell wall components have been discussed to mask fungal

**Figure 7.** (continued).

as diagonal lines, whereas stationary signals are vertical lines. Note that some signals persistently move over >20 μm. Time and distance is given in micrometers and seconds.

**(F)** Kymographs showing tip-directed motility of $G_3Mcs1^{\Delta 57\text{-}753}$-bound vesicles (ΔMM). Time and distance is given in micrometers and seconds.

**(G)** Kymographs showing motility of $G_3$Mcs1-bound vesicles in the presence of the F-actin inhibitor LatA (10 μM) and the microtubule inhibitor benomyl (30 μM). Time and distance is given in micrometers and seconds.

**(H)** Bar charts showing motility parameters in cells that were treated with the F-actin inhibitor LatA or the solvent DMSO. P values of Student's *t* tests are given above bars. Double asterisk indicates significance at $P < 0.001$. All bars are given as mean ± SE of 20 to 44 cells from one experiment. All results were confirmed by a second nonquantitative experiment.

hyphae to prevent recognition by the plant immune system (O'Connell and Panstruga, 2006; Rappleye et al., 2007; Fujikawa et al., 2009), and their absence from mutant hyphae might significantly impair the ability of the fungus to escape the plant defense system. Consequently, *mcs1* mutant infection is blocked due to disturbed hyphal development and an insufficient suppression of plant defense. A similar role of ChsV in protection of the invading hypha was reported in *F. oxysporum.* Here, deletion of a ChsV led to increased sensitivity to plant defense compounds, such as phytoanticipin or $H_2O_2$ (Madrid et al., 2003), and it was reported that ChsV null mutants induce plant defense (Pareja-Jaime et al., 2010). Taken together, the data demonstrate that class V CHSs perform essential roles during infection by sheltering the fungus against plant recognition.

### Mcs1-Bound Vesicles Rapidly Move along Microtubules

In this study, we show that polar localization of Mcs1 depends on its MMD and an intact actin cytoskeleton. This is in agreement with studies in budding yeast, the human pathogen *W. dematitidis*, and the filamentous ascomycete *A. nidulans*, where a role of F-actin and associated myosin in CHS delivery was shown (Santos and Snyder, 1997; Takeshita et al., 2005; Abramczyk et al., 2009). In contrast with these reports, here, we visualized the transport process itself. To our surprise, this approach revealed that long-range motility of $G_3$Mcs1-bound vesicles is a microtubule-dependent process. These structures are likely to be transport vesicles, which might correspond to the biochemically well-defined chitosomes (Bartnicki-Garcia, 2006). It is widely assumed that the microtubule cytoskeleton mediates delivery of CHS-bound vesicles to the growing hyphal apex (Takeshita et al., 2005; Bartnicki-Garcia, 2006; Steinberg, 2007), and microtubules are indeed known to support hyphal extension (Fuchs et al., 2005; Horio and Oakley, 2005). In *U. maydis* and *A. nidulans*, the microtubule plus ends are directed to the hyphal tip (Zhang et al., 2003; Konzack et al., 2005; Schuchardt et al., 2005), suggesting that presumably kinesin motor proteins take $G_3$Mcs1-bound vesicles to the growth region. The high transport

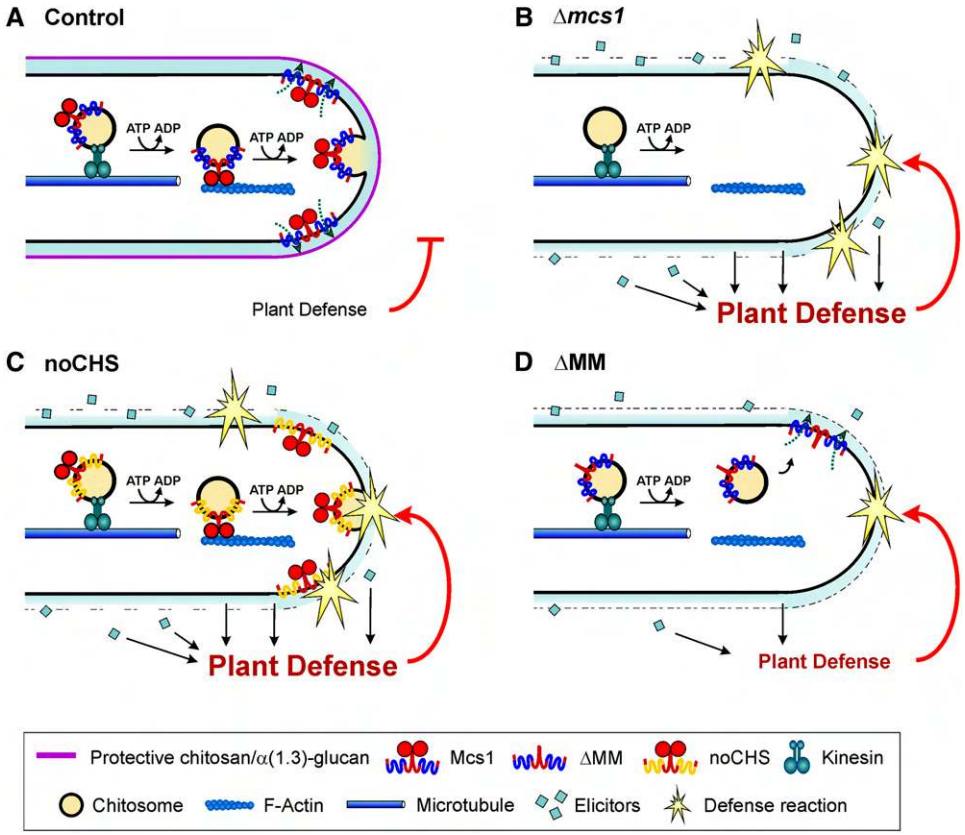


**Figure 9.** Model Suggesting a Role of Mcs1 during Plant Infection.

**(A)** Control: Mcs1 and presumably unknown kinesin motors cooperate in delivery of $G_3$Mcs1-bound vesicles. Due to intact cell wall architecture eliciting cell wall components are masked by protecting components, like chitosan or α(1,3)-glucan. Consequently, the plant defense system is not activated.
**(B)** Δ*mcs1*: Deletion of *mcs1* causes defects in cell wall architecture, which might trigger release of defense-eliciting cell wall compounds and therefore promote plant defense reactions.
**(C)** noCHS: Without CHS activity Mcs1 cannot build a proper cell wall. Elicitors are released that trigger the oxidative burst and hypersensitive reaction.
**(D)** ΔMM: Without the MMD the class V CHS is inefficiently exocytosed. Therefore, only reduced amounts of the truncated CHS can participate in cell wall formation, which lowers the effect on the cell wall architecture and the release of elicitors.

velocity of these vesicles (~1.8 μm/s) corresponds well with the velocity of kinesin-dependent organelle motility in fungal cells (1.5 to -2.0 μm/s; Steinberg and Schliwa, 1993; Steinberg, 1997). However, we also found that F-actin is required for $G_3$Mcs1 motility. This suggests that additional myosin motors participate in vesicle delivery. How both transport systems cooperate and which motors are responsible for delivery of the myosin CHS remain to be investigated.

### What Is the Role of Mcs1 in Delivery of Vesicles?

CHSs containing a MMD are not encoded by the genomes of the yeasts *S. cerevisiae* and *Schizosaccharomyces pombe* but were reported for numerous filamentous fungi, including the human pathogens *Cryptococcus neoformans*, *W. dermatitidis*, *Paracoccidioides brasiliensis*, and *Coccidioides posadasii* (Liu et al., 2004; Banks et al., 2005; Mandel et al., 2006; Nino-Vega et al., 2009) as well as the plant pathogens *Magnaporthe grisea*, *C. graminicola*, *G. zeae*, *Blumeria graminis*, *F. oxysporum*, and *U. maydis* (Park et al., 1999; Zhang and Gurr, 2000; Madrid et al., 2003; Weber et al., 2006; Werner et al., 2007; Kim et al., 2009). It was suggested that the membrane-bound ChsV transports itself to sites of exocytosis (Fujiwara et al., 1997; Madrid et al., 2003; Abramczyk et al., 2009). In this study, we show that motility of $G_3$Mcs1-carrying vesicles occurs in the absence of the MMD and that microtubules support long-range transport of these vesicles (Figure 9A). However, in the absence of F-actin, motility was clearly reduced and the apical accumulation of Mcs1 was abolished, suggesting cooperation of both transport systems.

Unconventional myosins are thought to cooperate with long-range transport along microtubules by delivering membranes over short distances (Langford, 1995; Brown et al., 2004). The motor domain of all ChsVs share important myosin motor signatures, including a P-loop and switch I and switch II loops, that are essential to function as an ATP-hydrolyzing mechanoenzyme (Takagi et al., 2004). In addition, we identified an IQ motif near the C-terminal end of the MMD of Mcs1 (amino acids 721 to 741; Calmodulin target Database, http://calcium.uhnres.utoronto.ca/ctdb/ctdb/sequence.html) and show here that this myosin CHS, like other myosin motors, dimerizes via a coiled-coil region located behind the motor domain. Thus, Mcs1 has all attributes known to be necessary for motility along F-actin. It is therefore tempting to speculate that Mcs1 mediates short-range motility of vesicles within the hyphal apex (Figure 9A). Alternatively, myosin CHSs might have a more stationary role and anchor cargo to the growth region, a concept previously suggested for CsmA in *A. nidulans* (Takeshita et al., 2005). This conclusion was supported by the observation that mutant CsmA proteins, carrying point mutations that are predicted to result in rigorously binding to F-actin (Ruppel and Spudich, 1996), localized at the hyphal apex (Takeshita et al., 2005). This localization strongly argues that the myosin CHS binds to F-actin only near the hyphal tip. In this study, we made use of a different mutant allele that also impairs the ATPase activity. However, in contrast with the mutations introduced by Takeshita et al. (2005), this mutation has been shown to abolish ATPase activity and F-actin binding in the presence of ATP (Ruppel and Spudich, 1996; Liu et al., 2001). This, in turn, suggests ATPase activity is required to anchor Mcs1 to the apical actin and, consequently, the mutant protein impaired in actin binding $G_3$Mcs1$^{E407K}$ (noATP) did not localize to the polar growth region.

### Conclusion

In this study, we showed that the CHS domain and the MMD of Mcs1 are essential for its function during pathogenicity. Our data are consistent with a model in which Mcs1-bound vesicles are delivered over long distances by microtubule motors, whereas the Mcs1 MMD supports short-range motility in the hyphal apex along F-actin (Figure 9A). The absence of the CHS in *mcs1*-null mutants most likely causes major defects in the fungal cell wall, which affects polarized growth and might elicit a hypersensitive response in colonized plant cells (Figure 9B). A similar situation could be observed in mutants expressing $G_3$Mcs1$^{D1436E/D1551E}$ (noCHS), suggesting that the cell wall defect triggers the plant defense reaction (Figure 9C). A truncated Mcs1 protein lacking the motor domain still reaches the apex but is rarely inserted into the plasma membrane (Figure 9D). As a consequence, hyphal growth occurs and the fungus can partially colonize the host tissue until a moderate plant response stops the infection (Figure 9D). Myosin CHSs are only found in filamentous fungi and, surprisingly, in bivalves (Weiss et al., 2006). Here, we show that they play a crucial role in a secretion pathway that is essential for virulence of plant and human fungal pathogens.

## METHODS

### Strains

The *Ustilago maydis* strains AB33, SG200, and SG200ΔMcs1 were described previously (Brachmann et al., 2001; Kämper et al., 2006; Weber et al., 2006). The genotypes of all strains used in this work are summarized in Table 1.

### Plasmids and Expression Constructs

All plasmids generated for this study were sequenced prior to transformation. Plasmids were designed for ectopic integration into the *ip* locus of *U. maydis*. pn3GMcs1 was obtained by exchange of the *otef* promoter of pOGMcs1 (Weber et al., 2006) by the endogenous promoter of *mcs1.* The *mcs1* promoter region was amplified using primers 5′-ACGGCGCG-CCCTCGGCTCGTGGCTTGAAGAG-3′ and 5′-GTCGGCGCGCCTATG-GCGACTTTGCGTACCAGG-3′ and ligated via *Asc*I to the pOGMcs1 backbone, which was amplified via inverse PCR using primers 5′-CGC-CGACAACATCATCCACGGG-3′ and 5′-CGCCGCAAGCTTCAGCTGC-TCGAG-3′. The single *egfp* was exchanged by a triple tandem repeat of *egfp* to the N terminus of *mcs1* via *Nco*I and *Nde*I, resulting in plasmid p3GMcs1. Plasmids pn$G_3$Mcs1$^{\Delta MM}$, pn3GMcs1$^{noAct}$, and pn$G_3$Mcs1$^{\Delta CC}$ were generated using pn$G_3$Mcs1 as template for inverse PCR and the following primers (1) p3GMcs1$^{\Delta MM}$, 5′-ATTCCCGTGTCAAGGTGTT-CCTTTC-3′ and 5′-TCCTGTTGCGGTTTCCAGACGAGGCG-3′; (2) p3GMcs1$^{noAct}$, 5′-TCGAGTGACTTGGAGGAGATGCCG-3′ and 5′-GAA-TTCCGATGCCGACGGTGCTTCGGAC-3′; and (3) p3GMcs1$^{\Delta CC}$, 5′-ATTCGCGCGGCGAATCGGACCC-3′ and 5′-TCGCCGTATGCGAA-AGGAACACC-3′. Plasmid pn3GMcs1$^{noATP}$ was generated using the QuikChange site-directed mutagenesis kit (Stratagene) and primers 5′-CTGTGTCAACTTTGCCTGCAAGAACCTTCACCGCTTCATGC-3′ and 5′-GCATGAAGCGGTGAAGGTTCTTGCAGGCAAAGTTGACACAG-3′; pn3GMcs1$^{noCHS}$ was obtained using the QuikChange multi site-directed

mutagenesis kit (Stratagene) and primers 5′-CGAGTACATTCTGCAGGT-CGAAGCCGATACCGAAGTTGAGGC-3′ and 5′-CTGCATCTGGGTGAA-GAGCGTTACCTGACGACGTTGGTGCTC-3′. For integration into the *ip* locus of *U. maydis*, all plasmids were linearized and transformed into *U. maydis* as described previously (Schulz et al., 1990). All homologous recombination were confirmed by DNA gel blot analysis. All molecular cloning followed standard procedures.

### Growth Conditions

All cultures of *U. maydis* were grown overnight at 28°C in complete medium (CM; Holliday, 1974) supplemented with 1% glucose or $YEPS_{light}$ (0.4% yeast extract, 0.4% peptone, and 2% sucrose), shaking at 200 rpm.

### Inhibitor Studies

For all inhibitor experiments, logarithmically growing cells were incubated with either 30 μM benomyl (stock: 10 mM in DMSO; Fluka), 10 μM LatA (stock: 20 mM in DMSO; kindly provided by Karen Tenney, University of California, Santa Cruz, CA), or 10 mM 2,3-butanedione monoxime (stock: 500 mM in water; Sigma-Aldrich). In control experiments, the corresponding amount of the solvent DMSO was used. The effectiveness of LatA and benomyl was tested using a strain expressing GFP-fimbrin (Castillo-Lluva et al., 2007) or GFP-α-tubulin (Steinberg et al., 2001). All cells were incubated on a rotation wheel for 30 to 45 min and for observation were placed on a 2% agarose cushion, supplemented with the respective drug.

### Protein Extraction and Immunodetection

Protein extraction and immunodetection was performed as described (Straube et al., 2001). For detection of GFP-labeled proteins, a monoclonal anti-GFP antibody was used (Roche Diagnostic). Loading controls were monitored using an antitubulin antibody (Calbiochem). In both cases, a secondary anti-mouse peroxidase-conjugated antibody was used (Cell Signaling). Chemiluminescence detection was done using the ECL Plus Western Blot detection reagent, following the manufacturer's instructions (GE Healthcare).

### Size Exclusion Chromatography

Superdex 200 10/300GL (GE Healthcare) was equilibrated in extraction buffer (10 mM HEPES, pH 7.5, and 50 mM NaCl). Cells were harvested by centrifugation and pellets were resuspended in 1 mL of extraction buffer, and cells were disrupted using a MP FastPrep-24 (MP Biomedical) three times for 60 s at 6.5 m/s. *U. maydis* cell extracts expressing HA-tagged HMcs1HN and HMcs1H were centrifuged for 30 min at 100,000*g* at 4°C. The respective supernatant (250 μL) was loaded on the column and eluted with buffer (10 mM HEPES and 500 mM NaCl) with a flow rate 0.5 mL/min using an Äkta FPLC system (GE Healthcare). For SDS-PAGE analysis, 50 μL SDS loading buffer was added to each fraction. HA-tagged Mcs1HN and Mcs1H from *U. maydis* (proteins HMcs1HN and HMcs1H, respectively) extracts run on the column were analyzed by immunoblotting using anti-HA antibody (1:10,000; Sigma-Aldrich). The column was calibrated with globular proteins of known size: vitamin $B_{12}$ (1.35 kD), myoglobin (17 kD), ovalbumin (44 kD), γ-globulin (158 kD), and thyroglobin (670 kD). The molecular weight was calculated on the basis of the determined calibration curve.

### Plant Pathogenicity Assays

Pathogenicity assays were performed as described (Kämper et al., 2006). For plant infections, cultures of the *U. maydis* strains were grown in $Yeps_{light}$ to an $OD_{600}$ of 0.8 to 1.0, centrifuged, resuspended in water to $OD_{600}$ = 3, and syringe injected into 7- to 8-d-old maize (*Zea mays*) seedlings (variety Early Golden Bantam; Olds Seeds). Disease symptoms were scored 12 d after infection as described (Molina and Kahmann, 2007).

### Quantitative Real-Time PCR

The fungal biomass in maize leaves was detected 8 d after infection. Three-centimeter sections of the third outer leaf were taken ~1 cm below the injection site. Surface attached fungal cells were removed by washing with an excess of water/0.1% Tween 20. For subsequent DNA extraction, 10 leaf sections were pooled and infected plant material was frozen in liquid $N_2$, followed by grinding and gDNA extraction as described (Hoffman and Winston, 1987). Quantitative real-time PCR analysis was performed using an iCycler (Bio-Rad) and the Platinum SYBR Green qPCR SuperMix-UDG (Invitrogen). Cycling conditions were 2 min 95°C, followed by 45 cycles of 30 s 95°C/30 s 61°C/30 s 72°C. Results were analyzed by iCycler software (Bio-Rad). Primers 5′-ACATCGTCAAGGC-TATCG-3′ and 5′-AAAGAACACCGGACTTGG-3′, detecting the *U. maydis* gene *um03726.1* (coding for a peptidyl-prolyl *cis-trans* isomerase; see accession number below), were used. For comparison with plant DNA, the maize housekeeping gene glyceraldehyde-3-phosphate dehydrogenase was amplified using GapDH-FW and GapDH-RV (5′-CTTCG-GCATTGTTGAGGGTTTG-3′ and 5′-TCCTTGGCTGAGGGTCCGTC-3′).

### Quantification of Immunoblots, Microscopy Data, and Real-Time PCR

For quantification of expression in immunoblots, experiments were repeated with three biological replicates and were blotted five times. Signals were detected using Medical X-ray Screen Films Blue Sensitive (CEA). Autoradiographs were taken at multiple exposure times to avoid signal saturation. Autoradiographs were scanned, signals were contrast inverted, and intensity was measured using MetaMorph software. The intensity of GFP signals was normalized by comparison with the α-tubulin loading control band in each lane. For quantification of real-time PCR results, three to nine independent infections were performed and total DNA extracted. Quantitative real-time PCR analysis was performed using this DNA as template. After each PCR, the specificity of the amplified product was verified, and the threshold cycle above background was calculated using Bio-Rad iCycler software. Normalization of the quantitative PCR data was performed by geometric averaging of internal control genes (Vandesompele et al., 2002). Relative amount of fungal DNA was then calculated from the ratio of amplified product of *U. maydis* peptidyl-prolyl *cis-trans* isomerase and maize glyceraldehyde-3-phosphate dehydrogenase using the Bio-Rad iCycler software. Microscopy images were analyzed using on raw 14 bit images using the MetaMorph software. For line scan analysis, the maximum intensity along two-pixel-wide lines of five hyphal tips was averaged. For quantitative DAB staining, raw images were transformed into grayscale images. The contrast was inverted, and the average signal intensity in the cell wall was measured using MetaMorph. All values were corrected for the background in the adjacent plant cells. All corrected values were plotted, and the average intensity values were calculated. All statistical analyses were done using Prism 4 software (GraphPad).

### Microscopy of Infected Plant Tissue

$H_2O_2$ production in plants was detected using DAB (Sigma-Aldrich) as described (Molina and Kahmann, 2007). Confocal microscopy of infected plant tissue was performed as described previously (Doehlemann et al., 2009). In brief, maize plant leaves were analyzed 3 d after infection using the third outer leaf at ~1 cm below the infection site. Plant leaves were destained in ethanol and incubated for 3 to 4 h at 85°C in 10% KOH.

Fungal hyphae were stained with 10 mg/mL wheat germ agglutinin-AF488 (Molecular Probes); plant cell walls were visualized using 1 mg/mL propidium iodide (Sigma-Aldrich)/0.02% Tween 20 for 30 min, followed by washing in PBS, pH 7.4. To visualize membranes in living plant tissue, leaf sections were stained with 4 μg/mL FM4-64/0.02% Tween 20 (Molecular Probes), and fungal material in planta was stained using wheat germ agglutinin-AF488 (Molecular Probes). Samples were observed using a TCS-SP5 confocal microscope (Leica). The plant cell wall was visualized by a 405-nm laser, and autofluorescence was detected at 415 to 460 nm. GFP fluorescence was excited at 488 nm and detected at 495 to 530 nm. Maximum projections of confocal Z-stacks were created using the Leica LAS-AF software package. Three-dimensional projections and movies were calculated with Imaris 6.3 software (Bitplane).

### Labeling of Cell Wall Components and Vacuoles

The α(1,3)-glucan staining was essentially done as described (Fujikawa et al., 2009). In brief, cells of strains SG200ΔMcs1, SG200$G_3$Mcs1, and SG200$G_3$Mcs1ΔMM were grown in complete medium/1% glucose at 28°C and fixed with 4% formaldehyde (EM-grade; Polyscience) for 30 min. After washing with an excess of PBS, cells were incubated for 1 h in PBS and supplemented with 3% milk powder, followed by treatment with 0.1 mg/mL mouse IgM MOPC-104E (Sigma-Aldrich) in PBS/0.3% milk powder for 1 h. After several washes in PBS, cells were incubated for 1 h in the secondary antibody (Cy3-conjugated anti-IgM; Jackson) in PBS/0.3% milk powder.

Chitosan staining was done modifying published protocols (Baker et al., 2007). Plants were infected with strains SG200$G_3$Mcs1 and SG200$G_3$Mcs1ΔMM, and leaves were harvested 3 d after infection. Small parts of the upper epidermis of infected leaves were removed using a fine forceps and immediately incubated in 4% formaldehyde/PBS for 2 h. The tissue samples were washed once and incubated in PBS/3% milk powder for 1 h. After washing several times in an excess of PBS, the samples were incubated for 2 h in PBS/250 μg/mL EosinY (Sigma-Aldrich; 5 mg/mL stock in DMSO). This was followed by two washes in PBS and incubation of the stained samples in PBS overnight at 4°C, which was necessary to remove unspecific background. Chitin was stained using rhodamine-conjugated wheat germ agglutinin (Sigma-Aldrich) as previously described (Weber et al., 2006). Vacuoles were stained with Cell-Tracker Blue (Molecular Probes) as described (Steinberg et al., 1998).

### Electron Microscopy

Liquid cultures were grown overnight, and cells were harvested by centrifugation at 6000 rpm for 3 min. Two to three microliters of the cell pellet was rapidly frozen at −182°C using a RMC JF-8000 Propane Jet Freezer (Boeckeler Instruments). Freeze substitution was done in a RMC FS-7500 (Boeckeler Instruments), using 0.1% uranyl acetate/0.1% glutaraldehyde in dried acetone at −90°C for 3d, followed by −30°C for 24 h. Cells were embedded in Lowicryl HM20 resin (Polysciences), and the sample was polymerized in BEEM capsules at −30°C in a Cryocut E (Leica), followed polymerization at room temperature for 48 h. Sections were cut at a thickness of 60 to 80 nm and placed on formvar-coated nickel grids. For detection of GFP epitopes, these grids were first treated with blocking buffer (0.2 μm filtered 1% BSA in PBS/0.05% Tween 20) for 30 min. This was followed by 3 h incubation in anti-GFP antibodies (mouse IgG monoclonal antibody; Roche Diagnostics; Living Colors polyclonal rabbit peptide antibody, Takara Bio Europe/Clontech; both diluted at 1:200 in blocking buffer). After several washes with PBS/0.05% Tween 20, the samples were incubated for 1 h in the secondary antibody (EM goat anti-mouse IgG, 10 nm gold; EM goat anti-rabbit IgG, 20-nm gold; BB International; both diluted at 1:20 in blocking buffer). After washing in buffer and water, samples were observed using a JEOL JEM 1400 electron microscope operating at 80 kV.

### Laser Epifluorescence Microscopy

For visualization of $G_3$Mcs1 and $G_3$Mcs1$^{\Delta 57\text{-}753}$, logarithmically growing cells of strain SG200$G_3$Mcs1 and SG200$G_3$Mcs1ΔMM were placed on a 2% agar cushion followed by immediate observation using a IX81 motorized inverted microscope (Olympus) equipped with a PlanApo ×100/1.45 Oil TIRF objective (Olympus). Excitation of fluorescently labeled proteins was performed using a VS-LMS4 laser merge system with solid-state lasers (488 nm, 70 mW; 561, 70mW; Visitron System). Laser intensity was controlled by a VS-AOTF100 system. Lasers were coupled into the light path using a VS-20 laser lens system (Visitron System). The laser output power was 18 to 24mW. For colocalization studies, a Dual-View Microimager (Optical Insights) was used that was equipped with an excitation dual line beam splitter (z491/561; Chroma), an emission beam splitter (565 DCXR; Chroma), an ET-Bandpass 525/50 (Chroma), and a BrightLine HC 617/73 (Samrock). All images were captured using a CCD camera (Photometric CoolSNAP HQ2; Roper Scientific). All parts of the system were under the control of the MetaMorph software (Molecular Devices). Samples were observed no longer than 10 min to prevent oxygen depletion. Images were processed and analyzed using MetaMorph.

To visualize $G_3$Mcs1 motility, the hyphal apex was photobleaching using a 405-nm/60-mW laser that was dimmed by a ND 0.6 Filter, resulting in ~15-mW output powers. The laser was controlled by UGA-40 controller (Rapp OptoElectronic) and VisiFRAP 2D FRAP control software for Meta Series 7.5.x (Visitron System). The laser was coupled into the light path using an OSI-IX 71 adaptor (Visitron System). Cells were radiated 75 ms at 80% laser power with a beam diameter of 30 pixels, followed by immediate observation using 200-ms exposure time and the 488-nm observation laser.

### Accession Numbers

Sequence data from this article can be found in the Arabidopsis Genome Initiative or GenBank/EMBL databases under the following accession numbers: Mcs1 (XP_759351), Syntaxin Sso1 (XP_760375), peptidyl-prolyl *cis-trans* isomerase (EAK84904), and glyceraldehyde-3-phosphate dehydrogenase (CAA33620.1).

### Supplemental Data

The following materials are available in the online version of this article.

**Supplemental Figure 1.** Colocalization of $G_3$Mcs1 and the Vacuoles, Stained with Cell-Tracker Blue.

**Supplemental Figure 2.** Localization of $G_3$Mcs1 in the Plasma Membrane.

**Supplemental Figure 3.** Analysis of the Putative Dimerization Domain of Mcs1.

**Supplemental Figure 4.** Immunoblot Analysis Showing Expression Levels of Mcs1 Mutant Proteins.

**Supplemental Figure 5.** DAB and FM4-64 Staining Fungi in Infected Plant Tissue.

**Supplemental Figure 6.** Staining of α(1,3)-Glucan in Cell Wall of Infectious Hyphae.

**Supplemental Movie 1.** Maize Leaf Tissue 3 d after Infection with *U. maydis mcs1*-Null Mutants.

**Supplemental Movie 2.** Maize Leaf Tissue 3 d after Infection with *U. maydis* Control Strains.

**Supplemental Movie 3.** Maize Leaf Tissue 3 d after Infection with *U. maydis* Mutants Lacking the MMD (Δ57-753).

**Supplemental Movie 4.** Motility of $G_3$Mcs1 Toward the Growth Region in a Hyphal Cell.

## ACKNOWLEDGMENTS

We thank M. Martin-Urdiroz for acquiring microscopy data, Justin Molloy for identifying the IQ motif in Mcs1, Natascha Steinberg for technical help with plant infection, Peter Splatt for technical support with electron microscopy, and Regine Kahmann for providing access to plant growth facilities. We also thank the anonymous reviewers for their constructive comments, which helped us to improve the manuscript. This work was supported by the Deutsche Forschungsgemeinshaft Graduate School 1216, a grant from the Biotechnology and Biological Science Research Council (BB/G00465X/1), and the Max-Planck Institute for Terrestrial Microbiology in Marburg.

Received February 26, 2010; revised June 26, 2010; accepted July 8, 2010; published July 27, 2010.

## REFERENCES

**Aalto, M.K., Ronne, H., and Keranen, S.** (1993). Yeast syntaxins Sso1p and Sso2p belong to a family of related membrane proteins that function in vesicular transport. EMBO J. **12:** 4095–4104.

**Abramczyk, D., Park, C., and Szaniszlo, P.J.** (2009). Cytolocalization of the class V chitin synthase in the yeast, hyphal and sclerotic morphotypes of *Wangiella* (Exophiala) *dermatitidis.* Fungal Genet. Biol. **46:** 28–41.

**Agrios, G.N.** (1997). Plant Pathology. (London: Academic Press).

**Baker, L.G., Specht, C.A., Donlin, M.J., and Lodge, J.K.** (2007). Chitosan, the deacetylated form of chitin, is necessary for cell wall integrity in *Cryptococcus neoformans.* Eukaryot. Cell **6:** 855–867.

**Banks, I.R., Specht, C.A., Donlin, M.J., Gerik, K.J., Levitz, S.M., and Lodge, J.K.** (2005). A chitin synthase and its regulator protein are critical for chitosan production and growth of the fungal pathogen *Cryptococcus neoformans.* Eukaryot. Cell **4:** 1902–1912.

**Bartnicki-Garcia, S.** (2006). Chitosomes: Past, present and future. FEM. Yeast Res. **6:** 957–965.

**Brachmann, A., Weinzierl, G., Kamper, J., and Kahmann, R.** (2001). Identification of genes in the bW/bE regulatory cascade in *Ustilago maydis.* Mol. Microbiol. **42:** 1047–1063.

**Brefort, T., Doehlemann, G., Mendoza-Mendoza, A., Reissmann, S., Djamei, A., and Kahmann, R.** (2009). *Ustilago maydis* as a pathogen. Annu. Rev. Phytopathol. **47:** 423–445.

**Brown, J.R., Stafford, P., and Langford, G.M.** (2004). Short-range axonal/dendritic transport by myosin-V: A model for vesicle delivery to the synapse. J. Neurobiol. **58:** 175–188.

**Castillo-Lluva, S., Alvarez-Tabares, I., Weber, I., Steinberg, G., and Perez-Martin, J.** (2007). Sustained cell polarity and virulence in the phytopathogenic fungus *Ustilago maydis* depends on an essential cyclin-dependent kinase from the Cdk5/Pho85 family. J. Cell Sci. **120:** 1584–1595.

**Chen, J., Zheng, W., Zheng, S., Zhang, D., Sang, W., Chen, X., Li, G., Lu, G., and Wang, Z.** (2008). Rac1 is required for pathogenicity and Chm1-dependent conidiogenesis in rice fungal pathogen *Magnaporthe grisea.* PLoS Pathog. **4:** e1000202.

**Chigira, Y., Abe, K., Gomi, K., and Nakajima, T.** (2002). *chsZ*, a gene for a novel class of chitin synthase from *Aspergillus oryzae.* Curr. Genet. **41:** 261–267.

**Choquer, M., Boccara, M., Goncalves, I.R., Soulie, M.C., and Vidal-Cros, A.** (2004). Survey of the *Botrytis cinerea* chitin synthase multigenic family through the analysis of six euascomycetes genomes. Eur. J. Biochem. **271:** 2153–2164.

**Doehlemann, G., van der Linde, K., Assmann, D., Schwammbach, D., Hof, A., Mohanty, A., Jackson, D., and Kahmann, R.** (2009). Pep1, a secreted effector protein of *Ustilago maydis*, is required for successful invasion of plant cells. PLoS Pathog. **5:** e1000290.

**Doehlemann, G., Wahl, R., Horst, R.J., Voll, L.M., Usadel, B., Poree, F., Stitt, M., Pons-Kuhnemann, J., Sonnewald, U., Kahmann, R., and Kamper, J.** (2008). Reprogramming a maize plant: Transcriptional and metabolic changes induced by the fungal biotroph *Ustilago maydis.* Plant J. **56:** 181–195.

**Fuchs, U., Manns, I., and Steinberg, G.** (2005). Microtubules are dispensable for the initial pathogenic development but required for long-distance hyphal growth in the corn smut fungus *Ustilago maydis.* Mol. Biol. Cell **16:** 2746–2758.

**Fujiwara, M., Horiuchi, H., Ohta, A., and Takagi, M.** (1997). A novel fungal gene encoding chitin synthase with a myosin motor-like domain. Biochem. Biophys. Res. Commun. **236:** 75–78.

**Fujikawa, T., Kuga, Y., Yano, S., Yoshimi, A., Tachiki, T., Abe, K., and Nishimura, M.** (2009). Dynamics of cell wall components of *Magnaporthe grisea* during infectious structure development. Mol. Microbiol. **73:** 553–570.

**Garcera-Teruel, A., Xoconostle-Cazares, B., Rosas-Quijano, R., Ortiz, L., Leon-Ramirez, C., Specht, C.A., Sentandreu, R., and Ruiz-Herrera, J.** (2004). Loss of virulence in *Ustilago maydis* by Umchs6 gene disruption. Res. Microbiol. **155:** 87–97.

**Hodge, T., and Cope, M.J.** (2000). A myosin family tree. J. Cell Sci. **113:** 3353–3354.

**Hoffman, C.S., and Winston, F.** (1987). A ten-minute DNA preparation from yeast efficiently releases autonomous plasmids for transformation of *Escherichia coli.* Gene **57:** 267–272.

**Holliday, R.** (1974). *Ustilago maydis*. In Handbook of Genetics, R.C. King, ed (New York: Plenum Press), pp. 575–595.

**Horio, T., and Oakley, B.R.** (2005). The role of microtubules in rapid hyphal tip growth of *Aspergillus nidulans.* Mol. Biol. Cell **16:** 918–926.

**Horiuchi, H., Fujiwara, M., Yamashita, S., Ohta, A., and Takagi, M.** (1999). Proliferation of intrahyphal hyphae caused by disruption of *csmA*, which encodes a class V chitin synthase with a myosin motor-like domain in *Aspergillus nidulans.* J. Bacteriol. **181:** 3721–3729.

**Kämper, J., et al.** (2006). Insights from the genome of the biotrophic fungal plant pathogen *Ustilago maydis.* Nature **444:** 97–101.

**Keon, J.P., White, G.A., and Hargreaves, J.A.** (1991). Isolation, characterization and sequence of a gene conferring resistance to the systemic fungicide carboxin from the maize smut pathogen, *Ustilago maydis.* Curr. Genet. **19:** 475–481.

**Kim, J.E., Lee, H.J., Lee, J., Kim, K.W., Yun, S.H., Shim, W.B., and Lee, Y.W.** (2009). *Gibberella zeae* chitin synthase genes, GzCHS5 and GzCHS7, are required for hyphal growth, perithecia formation, and pathogenicity. Curr. Genet. **55:** 449–459.

**Konzack, S., Rischitor, P.E., Enke, C., and Fischer, R.** (2005). The role of the kinesin motor KipA in microtubule organization and polarized growth of *Aspergillus nidulans.* Mol. Biol. Cell **16:** 497–506.

**Lamb, C., and Dixon, R.A.** (1997). The oxidative burst in plant disease resistance. Annu. Rev. Plant Physiol. Plant Mol. Biol. **48:** 251–275.

**Langford, G.M.** (1995). Actin- and microtubule-dependent organelle motors: Interrelationships between the two motility systems. Curr. Opin. Cell Biol. **7:** 82–88.

**Latge, J.P.** (2007). The cell wall: A carbohydrate armour for the fungal cell. Mol. Microbiol. **66:** 279–290.

**Levine, A., Tenhaken, R., Dixon, R., and Lamb, C.** (1994). $H_2O_2$ from the oxidative burst orchestrates the plant hypersensitive disease resistance response. Cell **79:** 583–593.

**Liu, G., Greenshields, D.L., Sammynaiken, R., Hirji, R.N., Selvaraj,**

**G., and Wei, Y.** (2007). Targeted alterations in iron homeostasis underlie plant defense responses. J. Cell Sci. **120:** 596–605.

**Liu, H., Kauffman, S., Becker, J.M., and Szaniszlo, P.J.** (2004). *Wangiella* (*Exophiala*) *dermatitidis* WdChs5p, a class V chitin synthase, is essential for sustained cell growth at temperature of infection. Eukaryot. Cell **3:** 40–51.

**Liu, X., Osherov, N., Yamashita, R., Brzeska, H., Korn, E.D., and May, G.S.** (2001). Myosin I mutants with only 1% of wild-type actin-activated MgATPase activity retain essential *in vivo* function(s). Proc. Natl. Acad. Sci. USA **98:** 9122–9127.

**Madrid, M.P., Di Pietro, A., and Roncero, M.I.** (2003). Class V chitin synthase determines pathogenesis in the vascular wilt fungus *Fusarium oxysporum* and mediates resistance to plant defence compounds. Mol. Microbiol. **47:** 257–266.

**Mandel, M.A., Galgiani, J.N., Kroken, S., and Orbach, M.J.** (2006). *Coccidioides posadasii* contains single chitin synthase genes corresponding to classes I to VII. Fungal Genet. Biol. **43:** 775–788.

**Martin-Udiroz, M., Madrid, M.P., and Roncero, M.I.** (2004). Role of chitin synthase genes in *Fusarium oxysporum.* Microbiology **150:** 3175–3187.

**Martin-Urdiroz, M., Roncero, M.I., Gonzalez-Reyes, J.A., and Ruiz-Roldan, C.** (2008). ChsVb, a class VII chitin synthase involved in septation, is critical for pathogenicity in *Fusarium oxysporum.* Eukaryot. Cell **7:** 112–121.

**Miyazaki, A., and Ootaki, T.** (1997). Multiple genes for chitin synthase in the zygomycete fungus *Phycomyces blakesleeanus.* J. Gen. Appl. Microbiol. **43:** 333–340.

**Molina, L., and Kahmann, R.** (2007). An *Ustilago maydis* gene involved in $H_2O_2$ detoxification is required for virulence. Plant Cell **19:** 2293–2309.

**Nagahashi, S., Sudoh, M., Ono, N., Sawada, R., Yamaguchi, E., Uchida, Y., Mio, T., Takagi, M., Arisawa, M., and Yamada-Okabe, H.** (1995). Characterization of chitin synthase 2 of *Saccharomyces cerevisiae*. Implication of two highly conserved domains as possible catalytic sites. J. Biol. Chem. **270:** 13961–13967.

**Nino-Vega, G.A., Sorais, F., and San-Blas, G.** (2009). Transcription levels of CHS5 and CHS4 genes in *Paracoccidioides brasiliensis* mycelial phase, respond to alterations in external osmolarity, oxidative stress and glucose concentration. Mycol. Res. **113:** 1091–1096.

**O'Connell, C.B., Tyska, M.J., and Mooseker, M.S.** (2007). Myosin at work: Motor adaptations for a variety of cellular functions. Biochim. Biophys. Acta **1773:** 615–630.

**O'Connell, R.J., and Panstruga, R.** (2006). Tête à tête inside a plant cell: Establishing compatibility between plants and biotrophic fungi and oomycetes. New Phytol. **171:** 699–718.

**Odenbach, D., Thines, E., Anke, H., and Foster, A.J.** (2009). The *Magnaporthe grisea* class VII chitin synthase is required for normal appressorial development and function. Mol. Plant Pathol. **10:** 81–94.

**Pareja-Jaime, Y., Martin-Urdiroz, M., Roncero, M.I., Gonzales-Reyes, J.A., and Ruiz-Roldan, M.C.** (2010). Chitin synthase-deficient mutant of *Fusarium oxysporum* elicits tomato plant defence response and protects against wild-type infection. Mol. Plant Pathol. **11:** 479–493.

**Park, I.C., Horiuchi, H., Hwang, C.W., Yeh, W.H., Ohta, A., Ryu, J.C., and Takagi, M.** (1999). Isolation of *csm1* encoding a class V chitin synthase with a myosin motor-like domain from the rice blast fungus, *Pyricularia oryzae.* FEMS Microbiol. Lett. **170:** 131–139.

**Pimentel, D., Lach, L., Zuniga, R., and Morriison, D.** (2000). Environmental and economic costs of nonindigenous species in the United States. Bioscience **50:** 53–65.

**Rappleye, C.A., Eissenberg, L.G., and Goldman, W.E.** (2007). Histoplasma capsulatum alpha-(1,3)-glucan blocks innate immune recognition by the beta-glucan receptor. Proc. Natl. Acad. Sci. USA **104:** 1366–1370.

**Ruiz-Herrera, J., and San-Blas, G.** (2003). Chitin synthesis as target for antifungal drugs. Curr. Drug Targets Infect. Disord. **3:** 77–91.

**Ruppel, K.M., and Spudich, J.A.** (1996). Structure-function studies of the myosin motor domain: importance of the 50-kDa cleft. Mol. Biol. Cell **7:** 1123–1136.

**Santos, B., and Snyder, M.** (1997). Targeting of chitin synthase 3 to polarized growth sites in yeast requires Chs5p and Myo2p. J. Cell Biol. **136:** 95–110.

**Sasaki, N., Asukagawa, H., Yasuda, R., Hiratsuka, T., and Sutoh, K.** (1999). Deletion of the myopathy loop of *Dictyostelium* myosin II and its impact on motor functions. J. Biol. Chem. **274:** 37840–37844.

**Schuchardt, I., Assmann, D., Thines, E., Schuberth, C., and Steinberg, G.** (2005). Myosin-V, Kinesin-1, and Kinesin-3 cooperate in hyphal growth of the fungus *Ustilago maydis.* Mol. Biol. Cell **16:** 5191–5201.

**Schulz, B., Banuett, F., Dahl, M., Schlesinger, R., Schafer, W., Martin, T., Herskowitz, I., and Kahmann, R.** (1990). The *b* alleles of *U. maydis*, whose combinations program pathogenic development, code for polypeptides containing a homeodomain-related motif. Cell **60:** 295–306.

**Sellers, J.R.** (2000). Myosins: A diverse superfamily. Biochim. Biophys. Acta **1496:** 3–22.

**Sietsma, J.H., Beth Din, A., Ziv, V., Sjollema, K.A., and Yarden, O.** (1996). The localization of chitin synthase in membranous vesicles (chitosomes) in *Neurospora crassa.* Microbiology **142:** 1591–1596.

**Soulie, M.C., Perino, C., Piffeteau, A., Choquer, M., Malfatti, P., Cimerman, A., Kunz, C., Boccara, M., and Vidal-Cros, A.** (2006). *Botrytis cinerea* virulence is drastically reduced after disruption of chitin synthase class III gene (Bcchs3a). Cell. Microbiol. **8:** 1310–1321.

**Steinberg, G.** (1997). A kinesin-like mechanoenzyme from the zygomycete *Syncephalastrum racemosum* shares biochemical similarities with conventional kinesin from *Neurospora crassa.* Eur. J. Cell Biol. **73:** 124–131.

**Steinberg, G.** (2007). Hyphal growth: A tale of motors, lipids, and the Spitzenkörper. Eukaryot. Cell **6:** 351–360.

**Steinberg, G., and Schliwa, M.** (1993). Organelle movements in the wild type and wall-less fz;sg;os-1 mutants of *Neurospora crassa* are mediated by cytoplasmic microtubules. J. Cell Sci. **106:** 555–564.

**Steinberg, G., Schliwa, M., Lehmler, C., Bölker, M., Kahmann, R., and McIntosh, J.R.** (1998). Kinesin from the plant pathogenic fungus *Ustilago maydis* is involved in vacuole formation and cytoplasmic migration. J. Cell Sci. **111:** 2235–2246.

**Steinberg, G., Wedlich-Soldner, R., Brill, M., and Schulz, I.** (2001). Microtubules in the fungal pathogen *Ustilago maydis* are highly dynamic and determine cell polarity. J. Cell Sci. **114:** 609–622.

**Straube, A., Enard, W., Berner, A., Wedlich-Soldner, R., Kahmann, R., and Steinberg, G.** (2001). A split motor domain in a cytoplasmic dynein. EMBO J. **20:** 5091–5100.

**Takagi, Y., Shuman, H., and Goldman, Y.E.** (2004). Coupling between phosphate release and force generation in muscle actomyosin. Philos. Trans. R. Soc. Lond. B Biol. Sci. **359:** 1913–1920.

**Takeshita, N., Ohta, A., and Horiuchi, H.** (2005). CsmA, a class V chitin synthase with a myosin motor-like domain, is localized through direct interaction with the actin cytoskeleton in *Aspergillus nidulans.* Mol. Biol. Cell **16:** 1961–1970.

**Takeshita, N., Yamashita, S., Ohta, A., and Horiuchi, H.** (2006). *Aspergillus nidulans* class V and VI chitin synthases CsmA and CsmB, each with a myosin motor-like domain, perform compensatory functions that are essential for hyphal tip growth. Mol. Microbiol. **59:** 1380–1394.

**Thordal-Christensen, H., Zhang, Z., Wei, Y., and Collinge, D.B.** (1997). Subcellular localization of $H_2O_2$ in plants. $H_2O_2$ accumulation in papillae and hypersensitive response during the barley-powdery mildew interaction. Plant J. **11:** 1187–1194.

**Tsuizaki, M., Takeshita, N., Ohta, A., and Horiuchi, H.** (2009). Myosin motor-like domain of the class VI chitin synthase CsmB is essential to

its functions in *Aspergillus nidulans.* Biosci. Biotechnol. Biochem. **73:** 1163–1167.

**Vandesompele, J., De Preter, K., Pattyn, F., Poppe, B., Van Roy, N., De Paepe, A., and Speleman, F.** (2002). Accurate normalization of real-time quantitative RT-PCR data by geometric averaging of multiple internal control genes. Genome Biol. **3:** 0034.1–0034.11.

**Weber, I., Assmann, D., Thines, E., and Steinberg, G.** (2006). Polar localizing class V myosin chitin synthases are essential during early plant infection in the plant pathogenic fungus *Ustilago maydis.* Plant Cell **18:** 225–242.

**Weber, I., Gruber, C., and Steinberg, G.** (2003). A class-V myosin required for mating, hyphal growth, and pathogenicity in the dimorphic plant pathogen *Ustilago maydis.* Plant Cell **15:** 2826–2842.

**Weiss, I.M., Schonitzer, V., Eichner, N., and Sumper, M.** (2006). The chitin synthase involved in marine bivalve mollusk shell formation contains a myosin domain. FEBS Lett. **580:** 1846–1852.

**Werner, S., Sugui, J.A., Steinberg, G., and Deising, H.B.** (2007). A chitin synthase with a myosin-like motor domain is essential for hyphal growth, appressorium differentiation, and pathogenicity of the maize anthracnose fungus *Colletotrichum graminicola.* Mol. Plant Microbe Interact. **20:** 1555–1567.

**Zhang, J., Li, S., Fischer, R., and Xiang, X.** (2003). Accumulation of cytoplasmic dynein and dynactin at microtubule plus ends in *Aspergillus nidulans* is kinesin dependent. Mol. Biol. Cell **14:** 1479–1488.

**Zhang, Z., and Gurr, S.J.** (2000). Walking into the unknown: A 'step down' PCR-based technique leading to the direct sequence analysis of flanking genomic DNA. Gene **253:** 145–150.

**Zheng, W., Zhao, Z., Chen, J., Liu, W., Ke, H., Zhou, J., Lu, G., Darvill, A.G., Albersheim, P., Wu, S., and Wang, Z.** (2009). A Cdc42 ortholog is required for penetration and virulence of *Magnaporthe grisea.* Fungal Genet. Biol. **46:** 450–460.